

1 **Variations in esker morphology and internal architecture record time-transgressive**
2 **deposition during ice margin retreat in Northern Ireland**

3 Ben J. Stoker^{1,2,*}, Stephen J. Livingstone¹, Iestyn D. Barr³, Alastair Ruffell⁴, Robert D. Storrar⁵,
4 Sam Roberson⁶

5 *Corresponding author, email address: stokerb@natur.cuni.cz

6 ¹ Department of Geography, University of Sheffield, UK, South Yorkshire, Sheffield, Winter Street,
7 S10 2TN

8 ² Department of Physical Geography and Geocology, Charles University, Prague, Czechia

9 ³ Department of Natural Sciences, Manchester Metropolitan University, UK, Manchester, Oxford Road,
10 M15 6BH

11 ⁴ School of Natural and Built Environment, Queens University Belfast, UK, Belfast, Elmwood Avenue,
12 BT7 1NN

13 ⁵ Department of the Natural and Built Environment, Sheffield Hallam University, UK, Sheffield,
14 Howard Street, S1 1WB

15 ⁶ Geological Survey of Northern Ireland, Dundonald House, Belfast, BT4 3SB, UK

16 Keywords: Eskers, Northern Ireland, morphology, sedimentology, deglaciation, meltwater

17 **Abstract**

18 The architecture and evolution of the subglacial hydrological system plays a key role in modulating
19 ice flow. Eskers provide an opportunity to understand subglacial hydrology at a broader perspective
20 than contemporary studies. Recent research has established a morphogenetic classification for eskers,
21 but these studies have been limited to topographically simple regions of a single ice sheet. We present
22 an updated map of esker distribution in Northern Ireland based on 5 m resolution elevation data. We
23 also present a high-resolution map of the glacial geomorphology of SW Northern Ireland, based on
24 ~0.4 m resolution elevation data. Ground Penetrating Radar data from four sites along the >20 km
25 long Evishanoran Esker system in central Northern Ireland are combined with geomorphological
26 observations to provide insight into depositional processes and controls on esker formation. Esker
27 architecture indicates two styles of deposition, including an initial high energy flow event in a
28 subglacial conduit, and delta foreset deposition close to the ice sheet margin following ice margin
29 retreat. These delta foreset deposits can be used to reconstruct the former ice margins. We identify
30 that local topographic complexity and geological structures (e.g. faults) are important controls on
31 esker formation. The broad-scale esker architecture remains the same despite variable esker planform
32 morphology, suggesting hydrological conditions alone cannot explain esker morphology. This study
33 provides further evidence that morphogenetic relationships cannot be based solely on remote sensing
34 data and must be supported by robust field data, especially where post-glacial processes may distort
35 esker morphology (e.g. peat infilling).

36

37 **1.0 Introduction**

38 The distribution of meltwater at the base of ice sheets influences ice motion by modulating basal sliding
39 and deformation of sediments. The influence of water on ice flow depends on the architecture of the
40 subglacial drainage network and how it evolves to accommodate water inputs (e.g. Budd et al., 1979;
41 Alley et al., 1986; Iken and Bindshadler, 1986). Efficient low-pressure networks of discrete channels
42 rapidly drain water to the margin and tend to reduce ice velocity (Hubbard and Nienow, 1997).
43 Inefficient distributed networks (e.g. linked cavities, canals and a porous till layer) result in increased
44 effective pressure, in turn leading to higher ice velocities (Röthlisberger, 1972; Schoof, 2010). Recent
45 observations from beneath the Antarctic and Greenland ice sheets have implicated dynamic subglacial
46 water systems in driving rapid ice-flow variations (Zwally et al., 2002; Bell et al., 2007; Stearns et al.,
47 2008; Bartholomew et al., 2010; Davison et al., 2019).

48 For investigations of subglacial hydrological processes, the imprint of meltwater drainage, recorded on
49 the beds of former ice sheets, has a clear advantage over data from contemporary ice sheets (e.g.
50 borehole surveys) because it is possible to reconstruct the history of meltwater drainage over centennial
51 to millennial time-scales and spatially over metres to hundreds of kilometres. These temporal and spatial
52 scales not only allow a more complete understanding of the architecture and evolution of the subglacial
53 drainage network but are relevant for informing numerical modelling experiments (cf. Greenwood et
54 al., 2016; Hewitt & Creyts, 2019). Eskers are the depositional imprint of drainage through subglacial
55 (R-channels), englacial or supraglacial channels (Price, 1969; Banerjee and McDonald, 1975;
56 Gustavson and Boothroyd, 1987; Brennand, 2000) and are commonly found across the beds of former
57 ice sheets (e.g. Storrar et al., 2014a; Stroeven et al., 2016; Clark et al., 2018). They typically comprise
58 elongate ridges of glaciofluvially deposited sand and gravel that can extend tens to hundreds of
59 kilometres, are usually arranged roughly parallel to former ice flow direction, and range from single
60 ridges to more complex anabranching forms (e.g. Flint, 1930; Brennand, 1994; Burke et al., 2012;
61 Storrar et al., 2015; Perkins et al., 2016). Esker geometry, distribution and sedimentary architecture
62 have been widely used to reconstruct drainage pathways and infer past ice sheet dimensions and
63 dynamics (e.g. Shreve, 1985; Dyke and Prest, 1987; Aylsworth and Shilts, 1989; Hebrand and Åmark,
64 1989; Clark and Walder, 1994; Brennand, 1994, 2000; Warren and Ashley, 1994; Margold et al., 2013;
65 Storrar et al., 2013, 2014a; Livingstone et al., 2015). However, there is still considerable uncertainty
66 over the genesis of eskers, including the extent to which they form time-transgressively or
67 synchronously (e.g. Brennand, 2000; Makinen, 2003; Cummings et al., 2011); the magnitude and
68 frequency of drainage (Burke et al., 2008, 2010, 2012; Livingstone et al., 2016; Drews et al., 2017);
69 and the vertical position in the ice mass (i.e. supraglacial, englacial or subglacial) in which they are
70 deposited (Price, 1969; Fitzsimmons, 1991; Perkins et al., 2016).

71 Understanding how eskers form is important for reconstructing palaeo-ice sheets and providing
72 information on subglacial hydrological processes. In particular, the varied form and architecture of
73 eskers is thought to be controlled by the hydrological properties of the channelised drainage system

74 (Burke et al., 2015; Storrar et al., 2015). For example, recent morpho-sedimentary studies of eskers in
75 southern Alberta, Canada, and mapping of eskers emerging from the front of Breiðamerkurjökull,
76 southeast Iceland, have related abundant meltwater and sediment supply to complex esker systems, and
77 low sediment supply and either high or low meltwater abundance to single ridges of uniform geometry
78 (Burke et al., 2015; Storrar et al., 2015, 2020). A barrier to understanding the formation of eskers at the
79 ice sheet-scale is the relative dearth of sedimentological investigations of these long esker systems.
80 Recent work (e.g. Burke et al., 2012; Perkins et al., 2013) has begun to address this using geophysical
81 investigations of the sedimentary architecture of eskers formed beneath the Cordilleran Ice Sheet. To
82 further investigate the relationship between ice sheet hydrology and esker properties, this paper
83 combines detailed geomorphological, geophysical and sedimentological data to assess controls on the
84 formation of a ~20 km long esker network in Northern Ireland (UK) whose morphology changes down-
85 flow from a complex multi-ridge system to a large single ridge.

86 **2.0 Background**

87 *2.1 Glacial history of Ireland*

88 The early stages of the onset of the Irish Ice Sheet (~ 35 ka) were characterised by incursion of Scottish
89 ice flowing in from the NE, which subsumed localised ice caps over Irish upland massifs (Colhoun,
90 1971; Clark and Meehan, 2001; Greenwood and Clark, 2009b). As Irish ice coalesced with western
91 Scottish ice, the location of the dominant ice dispersal centres migrated to upland areas in the west of
92 Ireland, exerting a strong control on ice flow patterns (Greenwood and Clark, 2009b). Heterogenous
93 growth patterns led to ice sheet sectors reaching their maxima at different times. For example, the
94 western margin reached its maximum position relatively early compared to the southern portion of the
95 ice sheet (Ó Cofaigh and Evans, 2007; Greenwood and Clark, 2009b; Ó Cofaigh et al., 2019). The
96 configuration of ice domes and the geomorphology of the Irish Ice Sheet required ice expansion onto
97 the continental shelf, with the Last Glacial Maximum (LGM; 23 ka – 18 ka) resulting in almost complete
98 terrestrial ice coverage across Ireland (Knight et al., 2004; Ó Cofaigh and Evans, 2007; Bradwell et al.,
99 2008; Greenwood and Clark, 2009a,b; Clark et al. 2018).

100 Deglaciation in Ireland was characterised by the migration of competing ice divides, which resulted in
101 a complex deglacial history (Knight, 2003, 2019; Greenwood, 2009b). The ice sheet fragmented as it
102 retreated into upland dispersal centres such as the Connemara Mountains in Western Ireland and County
103 Donegal to the north (Wilson *et al.*, 2019), or lowland ice domes situated in the Lough Neagh Basin
104 and Omagh Basin (Fig. 1). Ice sheet retreat is thought to have been interspersed with asynchronous
105 phases of localised ice advance or stagnation, likely related to the migration of ice divides (Knight,
106 1999; Knight, 2006; Clark *et al.*, 2012; Callard et al., 2020; Chiverrell *et al.*, 2020). Within central
107 Northern Ireland, the two dominant LGM ice dispersal centres were situated in the Lough Neagh basin,
108 and in the Sperrin Mountain range to the north (Fig. 1) (Knight, 1999). During this period, SW ice flow
109 dominated from an ice dome in the NE Omagh Basin offshore towards Donegal Bay (Fig. 1), indicated

110 by an area of subglacial ribs across the Omagh Basin (Knight and McCabe, 1997). Subglacial ribs across
111 central Northern Ireland often display modification or drumlinisation likely associated with changes in
112 ice flow patterns and subglacial thermal regime (Knight, 1997; Knight and McCabe, 1997). An ice flow
113 reversal occurred during deglaciation when the dominant ice dome over the Omagh Basin migrated SW
114 to the Lower Lough Erne Basin, leading to NE ice flow forming a prominent esker system overlying
115 the subglacial ribs (Knight, 2004). The regional retreat pattern to the SW is documented by a series of
116 meltwater landforms, including eskers. A glacial lake formed between the retreating ice sheet margin
117 and the Sperrin Mountains to the north, resulting in the formation of a series of deltas (Dardis, 1986).
118 The final stages of deglaciation were characterised by localised mountain ice caps, with the last
119 remnants of the Irish Ice Sheet likely located in the mountains of Donegal in the northwest (Greenwood
120 and Clark, 2009b; Smith and Knight, 2011).

121 Research into the meltwater systems of Ireland has a long history stretching back to the late 19th century,
122 and has concentrated on the origin of the large (up to 50 m high) ridges of the Esker Riada system in
123 the Irish Midlands (Sollas, 1896; Gregory, 1912, 1921; Hinch, 1921; Flint, 1930). Theories on the origin
124 of these eskers revolved around whether they were deposited by a sub- or supraglacial river system, or
125 whether they represented deltaic glaciofluvial deposits (Gregory, 1921). More recently, studies have
126 debated whether the Esker Riada system and associated glaciofluvial sediments were deposited by
127 meltwater in an interlobate position, between two retreating ice masses (Warren and Ashley, 1994;
128 Pellicer et al., 2012), or as part of a multi-phase model involving westerly ice sheet retreat, followed by
129 a period of ice sheet readvance from the north (Delaney, 2001a, b, 2002; Delaney et al., 2018). The
130 eskers of central Northern Ireland have been used to reconstruct the migration of ice domes and time-
131 transgressive variations in the subglacial drainage system (Knight, 1997; 2019), but historically, there
132 has been less research focused on them.

133 *2.2 Regional Context and Landform Distribution*

134 Central Northern Ireland incorporates the Sperrin Mountains to the north and the Omagh Basin; a low
135 elevation region of undulating topography, to the south (Fig. 1). The regional geology is varied, with a
136 series of folded and faulted Palaeozoic sandstones and limestones to the south, and crystalline granites
137 and gabbros to the north, with varying degrees of metamorphism across the Tyrone Igneous Complex
138 (Knight, 1997; Chew *et al.*, 2008; Geological Survey Northern Ireland, 2016). A series of three large,
139 subparallel fault lines trend NE-SW and define geological boundaries, while smaller faults with a
140 variety of orientations are also prevalent (Geological Survey Northern Ireland, 2016).

141 A range of glacial landforms have been documented across the region, including meltwater channels,
142 eskers, drumlins and subglacial ribs (Colhoun, 1970; Knight, 2003; Clark et al., 2018). Major moraines
143 are largely absent across central Northern Ireland, being restricted to the present coastline and the
144 continental shelf onto which the Irish Ice Sheet extended (Clark et al., 2018; Ó Cofaigh et al., 2019).
145 An area of subglacial ribs dominates the lowland areas across Central Northern Ireland, with ridge

146 crestlines oriented perpendicular to SW ice flow during the LGM (Knight and McCabe, 1997; Knight,
147 2002). These subglacial ribs are commonly drumlinised or exhibit modification by meltwater, which
148 may have been stored in the lowland area between ridge crestlines (Knight and McCabe, 1997; Knight,
149 2002, 2006). Alongside subglacial ribs, E-W orientated drumlins dominate the lowlands of the Omagh
150 and Lough Erne basins (Knight, 1997, 2003). A prominent esker system located NE of the Lower Lough
151 Erne Basin forms a series of bifurcating ridges in a meltwater valley dissecting the zone of subglacial
152 ribs (Fig. 2a). This system was deposited under NE ice flow during deglaciation to the SW, contrasting
153 with the SW ice flow responsible for the formation of the subglacial ribs (Knight, 2002). Therefore,
154 these eskers represent a reversal of the hydraulic gradient as the ice dome situated over the Omagh
155 Basin migrated towards the Lower Lough Erne Basin (Knight and McCabe, 1997).

156 The present study focuses on a >20 km long complex esker system in County Tyrone, Central
157 Northern Ireland. The esker complex trends out of three meltwater channels cutting through the
158 Fintona Hills to the south, and terminates near the Sperrin Mountains in the north (Figs. 1, 2 and
159 3). The NE sector was mapped in part by Gregory (1925) and termed the Evishanoran Esker. Early
160 debate sought to identify whether deposition was associated with local ice masses from the east, or
161 a larger ice mass from the southwest (Charlesworth, 1926; Gregory, 1926). Here we refer to the
162 entire esker complex as the Evishanoran Esker, including newly mapped segments that were not
163 documented in Gregory (1925). A series of eskers to the SW in the Fintona Hills were likely
164 deposited during a later stage of deglaciation and form a meltwater routeway with the Evishanoran
165 Esker (Knight, 2019).

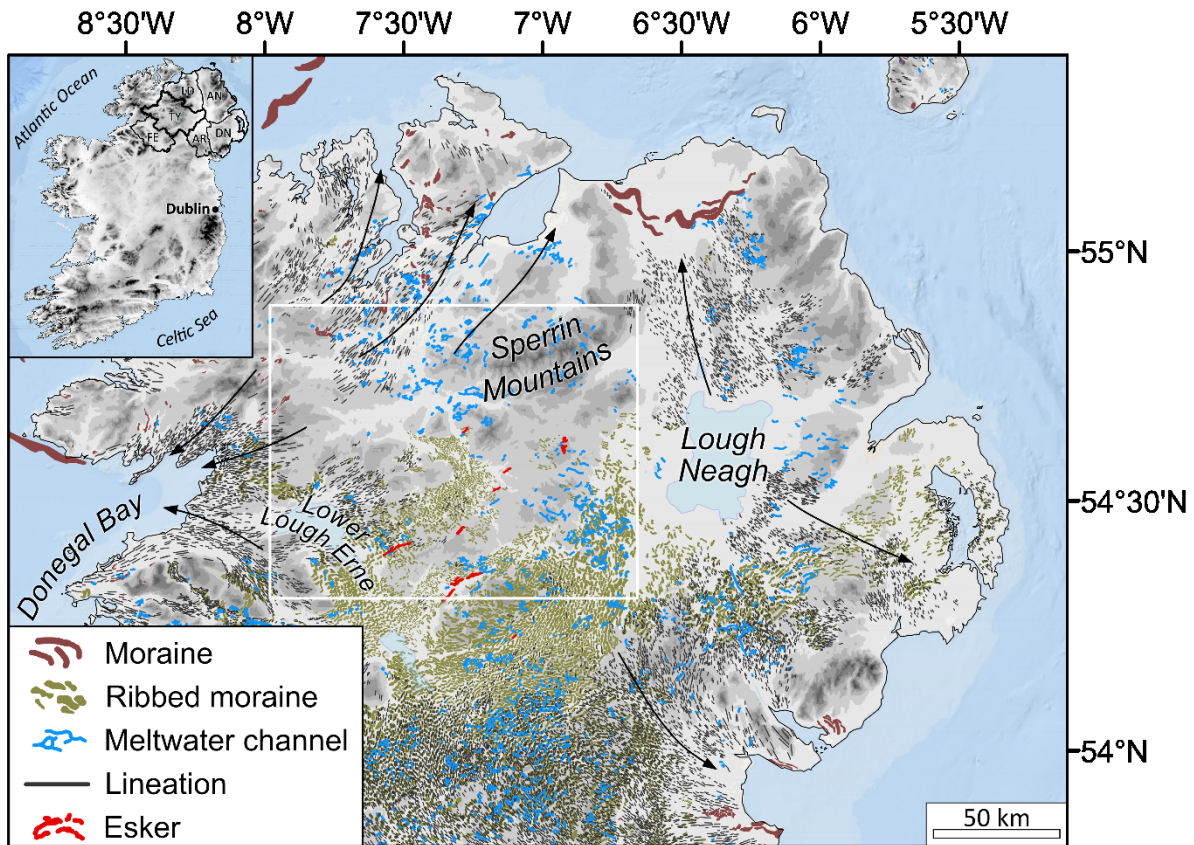
166 **3.0 Methods**

167 *3.1 Geomorphological mapping*

168 Comprehensive mapping of esker ridges was undertaken for the whole of Northern Ireland. Landform
169 mapping was performed within ArcGIS 10.4.1, using a 5 m resolution digital elevation model (DEM)
170 produced by the Land and Property Services Northern Ireland under MOU205, provided to Queens
171 University Belfast. We also mapped all glacial landforms across the study area of SW Northern Ireland
172 using a ~0.4 m resolution digital surface model (DSM) to provide geomorphological context of the area
173 surrounding the Evishanoran Esker (Fig. 2).

174 Landform identification was based on morphology, association with other features and local
175 topography. Esker crestlines were digitized as polylines to investigate their broad-scale distribution and
176 morphological characteristics. Fan-shaped enlargements located at esker termini were classified as
177 esker fans and digitized as polygons at the break of slope. The thalwegs of meltwater channels were
178 digitized as polylines and classified as either subglacial or lateral according to the criteria set out by
179 Greenwood *et al* (2007). All subglacial bedforms were mapped as polygons, including: subglacial ribs
180 (ribbed moraine), drumlins, mega-scale glacial lineations, and streamlined bedrock features. Our
181 mapping builds on earlier low-resolution mapping from Landsat and SPOT satellite imagery and field

182 surveys (Knight, 2003; Greenwood and Clark, 2009a), and has resulted in the creation of a
 183 comprehensive database of Northern Irish eskers, consistent with the NextMap 5 m resolution data used
 184 for the rest of the UK (Clark et al., 2018), and detailed mapping of glacial landforms in SW Northern
 185 Ireland at 0.4 m resolution.



186
 187 Figure 1. The distribution of mapped glacial landforms within the BRITICE v2 database across
 188 Northern Ireland (Clark *et al.*, 2018). Lineations include Mega-Scale Glacial Lineations (MSGSL) and
 189 drumlins. Major ice flow directions during the LGM are indicated by the black arrows. The white box
 190 indicates the study area.

191 *3.2 Ground Penetrating Radar*

192 Ground Penetrating Radar (GPR) data were acquired in August and November 2016. A total of ~1.8
 193 km are presented here, including profiles along the crestlines of the eskers and cross profiles in a range
 194 of topographic contexts and for different esker forms. A 32-bit Mala Ground Explorer (GX) controller
 195 unit connected directly to a 160MHz GX shielded antenna on a rough terrain skid plate was used in
 196 August 2016. Radar profiles were acquired at a constant walking pace in a continuous, time-triggered
 197 shot mode using hyperstacking to reduce random noise. A Mala Ramac system consisting of a 4 m-long
 198 Rough Terrain Antenna, comprising in-line, unshielded transmitting and receiving antennas with a 1.5
 199 m spacing and 100MHz centre frequency was used in November 2016. Collection of radar data was
 200 performed at a constant walking pace, in a time-triggered mode, with 16 stacks at a delay of 0.5-seconds.

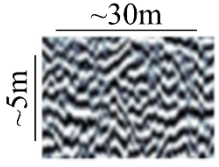
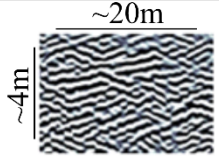
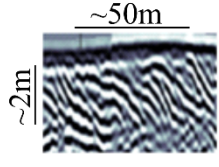
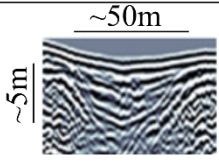
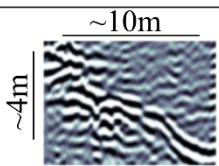
201 All radar survey lines were simultaneously mapped using a Leica CS15 differential Global Positioning
202 System (dGPS) unit to topographically correct the profiles.

203 Processing of radar data was performed within REFLEXW v7.5.9, the proprietary software of Karl
204 Sandmeier under licence number 401 provided to Queen's University, Belfast. A standard processing
205 sequence was developed, using the following steps: static correction of time-zero drift, removal of low
206 frequency signal saturation (dewow), application of gain to increase the visibility of reflections at depth,
207 diffraction stack migration, background removal to reduce antenna ringing, bandpass filtering and
208 topographic correction with the associated dGPS trace, finally radargrams were plotted in MatLab
209 v9.1.0.441655 (Neal, 2004; Cassidy and Jol, 2009). A velocity of 0.1 m/ns for migration was used,
210 consistent with exposures of eskers in sand extraction pits, hillside scars and road-cuts (see section 3.3)
211 (Russell et al., 2001; Pellicer et al., 2012; Livingstone et al., 2016). GPR profiles were interpreted by
212 identifying high-amplitude reflectors indicative of bounding surfaces between radar facies. Six radar
213 facies (*sensu* Gawthorpe *et al.*, 1993) were differentiated based upon depositional characteristics,
214 including associations with sediment facies identified from exposures in the field and the broad
215 characteristics of reflectors within a unit (Table 1). Lateral discontinuities and offset reflectors were
216 interpreted as geological faults (e.g. Fiore et al., 2002).

217

218 3.3 Sedimentology

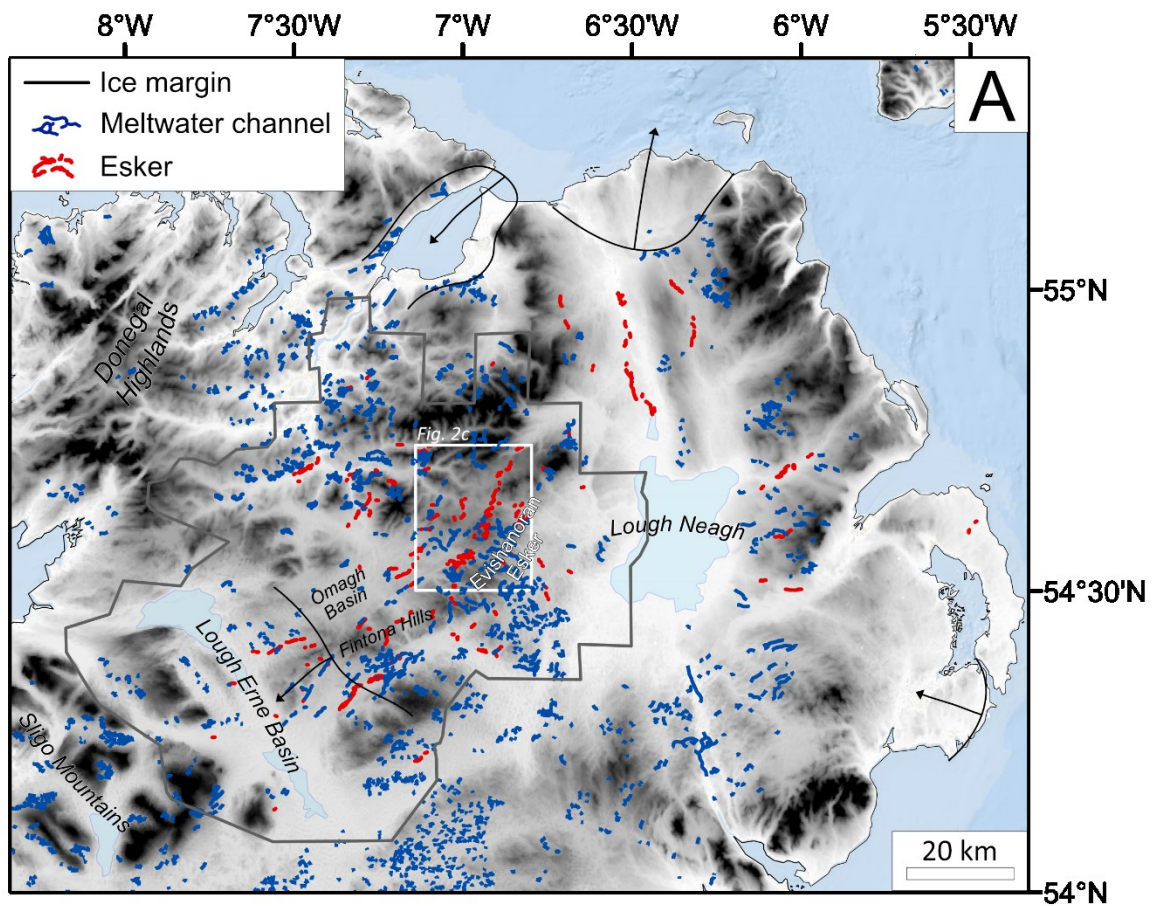
219 Gravel pit exposures adjacent to, and below, the GPR profiles were investigated to provide an insight
220 into the flow conditions responsible for ridge formation in the Evishanoran Esker, and to provide
221 ground-truthing for the interpretation of radargrams. Four sediment exposures were logged within the
222 complex, multi-ridge system and the simple, single-ridge system (Fig. 2). Scaled sediment logs were
223 drawn to record stratigraphic data, including details on the sedimentary structures, texture, and the unit
224 characteristics, such as bed geometry and contacts. Lithofacies were based on Evans and Benn (2004).
225 Clast macrofabric and palaeoflow indicators (e.g. ripples) supplemented stratigraphic logs (Miall,
226 1985).

Facies type	Radar facies example	Facies characteristics	Facies interpretation
Esker ridge facies		Radar Facies 1: Chaotic, discontinuous reflectors.	Coarse gravel deposited subglacially under high flow velocities (Burke <i>et al.</i> , 2015)
		Radar Facies 2: Sub-horizontal moderately continuous reflectors	Vertical accretion of sandy material (Burke <i>et al.</i> , 2012)
		Radar Facies 3: Low-angle dipping reflections	Delta foresets composed of sand and gravel (Burke <i>et al.</i> , 2010)
		Radar Facies 4: Concave-up, bowl-shaped reflectors	Erosional trough fills (Perkins <i>et al.</i> , 2016)
Post-glacial facies		Radar Facies 5: Attenuated, horizontal reflections	Post-glacial peat infill (Jol and Smith, 1991)

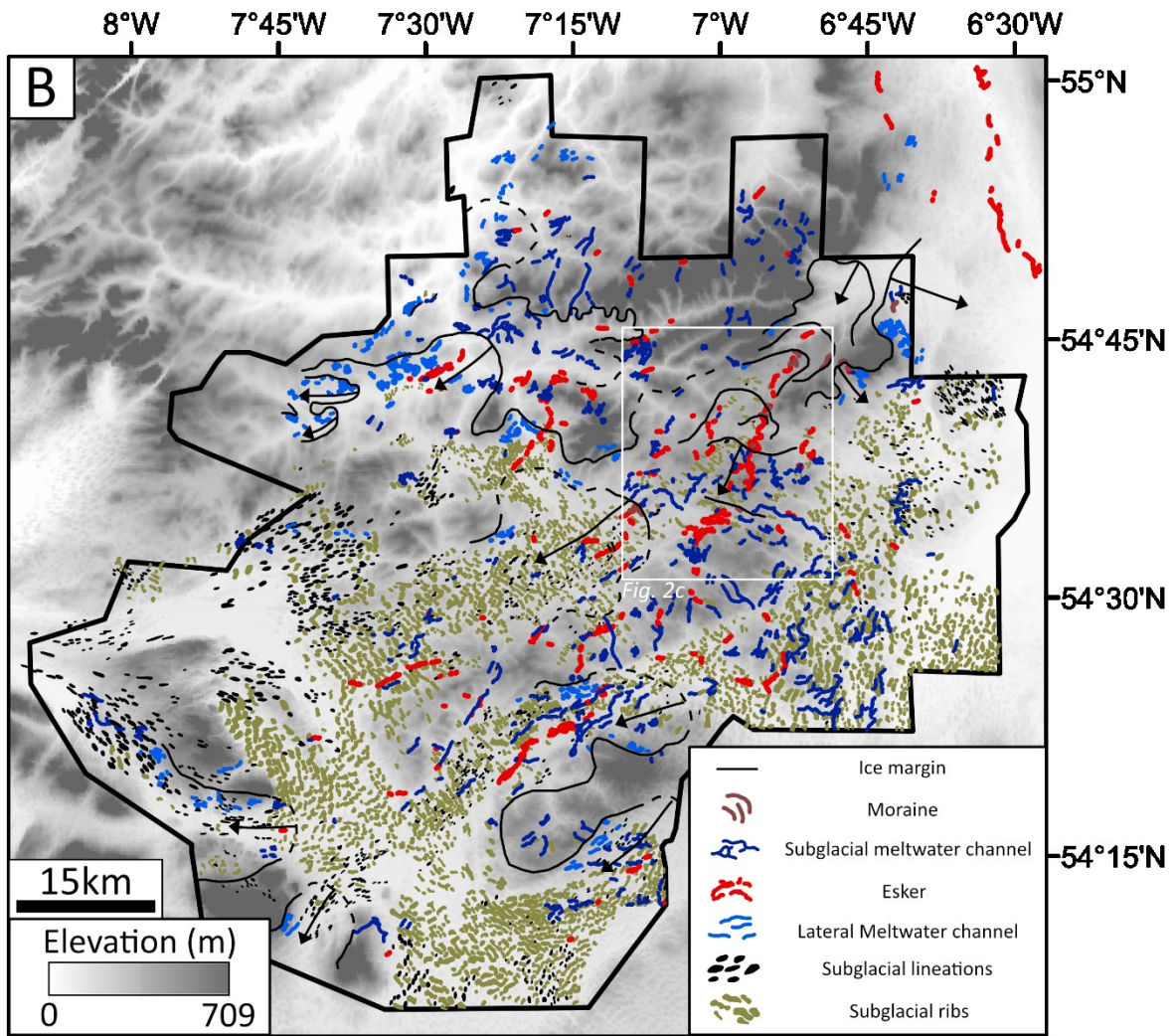
227

228 Table 1. Summary of key radar facies observed along the Evishanoran Esker, including both
 229 glaciofluvial and post-glacial features. Further description and interpretation of radar facies is presented
 230 in section 4.2.1.

231



232
 233 Figure 2. (a) An updated map of the meltwater landforms of Northern Ireland, including features
 234 mapped in this study. Meltwater channels from the BRITICE v2 compilation are also included (Clark
 235 *et al.*, 2018). Note the occurrence of a large esker system to the west of Lough Neagh, unreported in the
 236 BRITICE database. Ice margin positions are adapted from Greenwood and Clark (2009b), with arrows
 237 showing ice margin retreat direction. The grey box indicates the extent of high-resolution (~0.4 m)
 238 DSM coverage used within this study and shown in Figure 2b.
 239



240

241

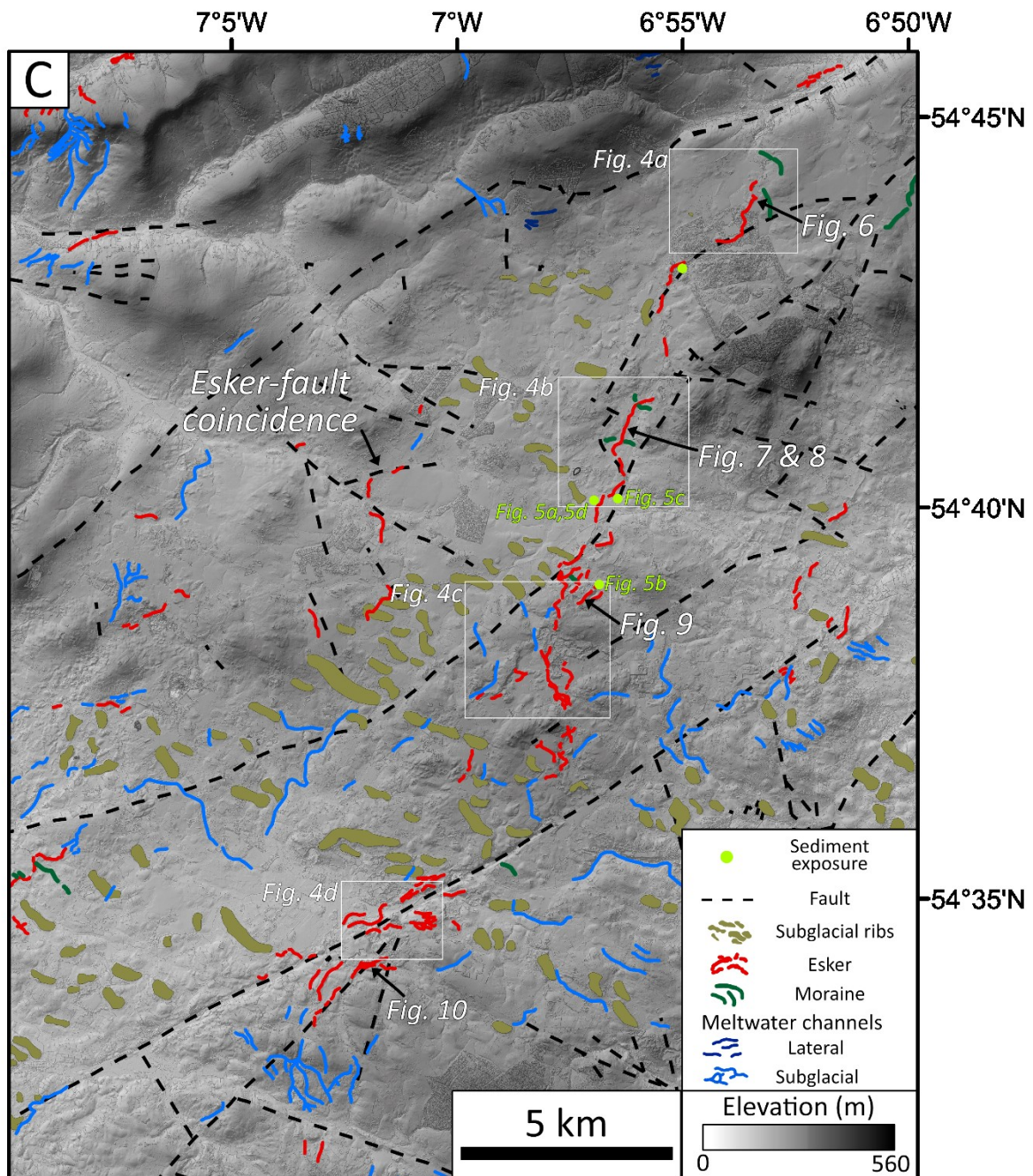
242

243

244

245

Figure 2. (b) Glacial geomorphology of SW Northern Ireland based on a 0.4m DSM. Schematic ice margin positions (black lines) have been drawn based on esker morphology, fan deposits, lateral meltwater channels and moraines. Dashed black lines indicate areas of lower certainty in ice margin position. Black arrows indicate ice margin retreat directions. The black outline indicates the extent of DSM coverage.



246
 247 Fig. 2. (c) The esker system in County Tyrone, annotated with the location of investigated sediment
 248 exposures. Note the coincidence of the southern esker system with a large SW-NE trending fault, while
 249 some eskers in the northwest demonstrate dramatic changes in orientation to follow fault lines. White
 250 boxes highlight features detailed within Fig. 4. Yellow text indicates which photographs from Fig. 5
 251 relate to each sediment exposure. Geological faulting data is based on the 10K geology dataset,
 252 reproduced with the permission of the Geological Survey of Northern Ireland. Crown Copyright 2018.

253 **4.0 Results and interpretations**

254 *4.1 Glacial Geomorphology*

255 A complete map of the glacial meltwater landforms of Northern Ireland is presented in Fig. 2a. The
 256 map contains 457 esker ridges, totalling 220 km in length, compared to 63 esker ridges (40 km) detailed

257 for this region in the BRITICE v2 database (Clark *et al.*, 2018). Esker distribution is heterogeneous,
258 with the majority concentrated along a NE-SW axis to the south of the Sperrin Mountains and a > 20
259 km long N-S trending esker system to the north of the Lough Neagh Basin. Meltwater channels most
260 commonly occur near upland regions (Fig. 2a). Meltwater channels have been documented by previous
261 mapping efforts and are ubiquitous across Northern Ireland (Charlesworth, 1924; Colhoun, 1970;
262 Knight, 2006; Greenwood and Clark, 2009a).

263 We present a detailed map of the glacial geomorphology of SW Northern Ireland in Fig. 2b, including
264 moraines, meltwater channels (lateral and subglacial), eskers and subglacial bedforms (lineations and
265 ribs). To the south of the Sperrin Mountains, a complex system of over 80 ridges form the Evishanoran
266 esker system, spanning > 20 km and demonstrating considerable variation in morphology over its length
267 (Fig. 2 and 3). The esker system is oriented SW-NE, broadly aligned with an area of subglacial ribs.
268 Across this region, further glaciofluvial landforms associated with the esker system are observed. Most
269 notably, the SW sector is associated with a series of subglacial meltwater channels cut into a slope that
270 trends against the regional northwards ice flow, fan-shaped deposits at the northern terminus of some
271 eskers, and a kame terrace on the southern slopes of the Sperrin Mountains. To the SW, the esker system
272 in the Fintona Hills likely forms a meltwater routeway with the Evishanoran Esker that was active
273 during later stages of deglaciation (Knight, 2019). We define three distinct esker sections based on
274 variations in esker planform; the northern sector of the esker is composed of a predominantly simple
275 system of single ridges, the central sector is dominated by a complex, arborescent ridge network
276 distributed around a hill (~100m relief), and the southern sector comprises a complex, anabranching
277 system of multiple subparallel ridges (Figs. 3, 4).

278 In the northern sector of the esker system (Fig. 4a,b), a simple planform dominates, consisting of nine
279 consecutive ridges, with a total length of ~9 km (Table 2). The esker system trends uphill towards the
280 NE, with ridges orientated along a uniform, broad valley bottom. However, the eskers in this sector are
281 morphologically complex. Some consecutive ridges are offset, while others terminate in fan-shaped
282 deposits at their northern end, or exhibit enlargements in the esker profile (Fig. 4b; Table 2). These
283 ridges display considerable variability in size; ranging from 25 to 80 m in width and from 5 to 15 m in
284 relief. We identify a series of six small moraine ridges across this sector, which record former ice margin
285 standstills. Three of the four esker enlargements and fan-shaped deposits are observed coincident with
286 moraines.

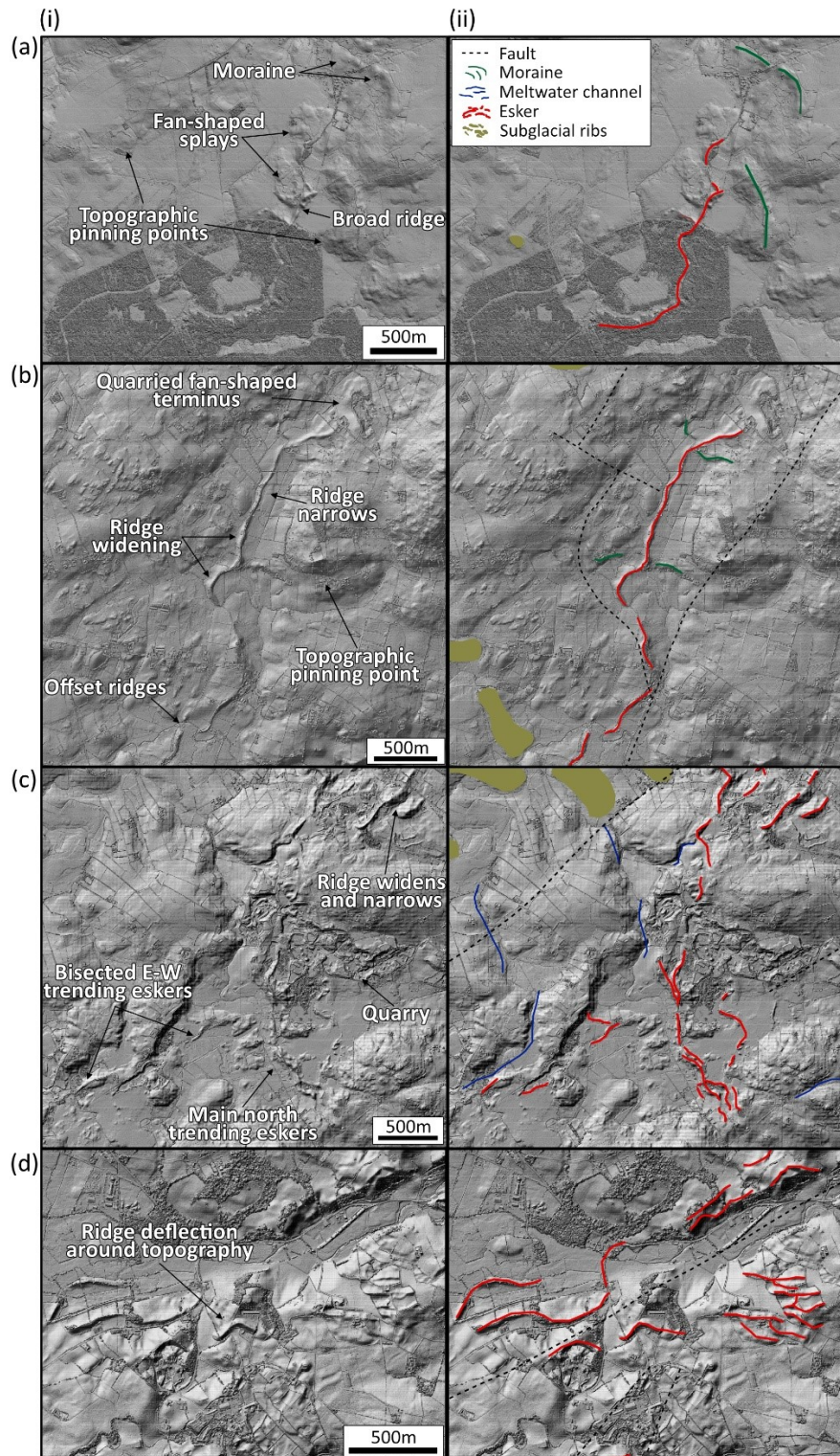


287

288 Figure 3. Photographs detailing the morphology of the Evishanoran Esker. (A) Looking east along a
 289 round-crested ridge within the complex, multi-ridge esker in the southern sector (54.571°N , -7.041°E).
 290 (B) An esker ridge ending in a fan-shaped deposit within the central sector of the esker complex, formed
 291 by water flow down the hill from the right of the image (54.650°N , -6.953°E). (C) A ridge along the
 292 Esker Road within the northern sector (54.683°N , -6.942°E). Radar surveys revealed peat infilling
 293 around the ridge, masking the true esker size. (D) Variations in ridge morphology towards the
 294 termination of the northern sector (54.734°N , -6.893°E).
 295

296 Further SW (central sector), the esker transitions into a complex, arborescent system of short ridges
 297 (~ 0.3 km long) with more subdued relief (~ 6 m). This coincides with a change to greater variability in
 298 relief in the surrounding topography (183 – 296 m a.s.l.) and a broadly downhill trend towards the NE.
 299 The southern end of the esker is split around a hill, with the western limb trending S-N before turning
 300 W-E, where it is cross-cut by the eastern limb, which trends N-S (Figs. 2a, 4c). The esker ridges within
 301 this sector display a simple morphology, with an enlargement only observed on a single ridge. We
 302 mapped a single moraine within this esker sector, which coincided with the esker enlargement.

303 The southern sector consists of multiple, subparallel ridges along a slope, which broadly trends downhill
 304 to the NE. While considerable variation in relief is observed due to the undulating terrain, cross-cutting
 305 relationships are absent within this sector, although ridges are observed to bifurcate (Fig. 4d). A single
 306 small esker enlargement is observed within this sector and a small moraine is present at the eastern end
 307 of the system.



308

309

310

311

312

313

314

Figure 4. Hillshaded DEM detailing key morphological characteristics of the Evishanoran Esker. (a) Widening of the esker ridge towards the terminus of the simple system in the northern sector, (b) Offset ridges at the initiation of the simple system in the northern sector, (c) Cross-cutting of east trending ridges by the main north trending ridge within the complex esker system in the central sector of the esker complex, (d) Deflection of ridges around a topographic obstacle (possible bedrock or earlier drumlin) within the southern sector.

315 Complex geological faulting is observed across the study region (Fig. 2). Esker ridges commonly occur
316 near faults, while some also change orientation to follow faultlines (GSNI, 2016) (Fig. 2). This is
317 illustrated by the large fault system towards the S of the region, which trends ENE-WSW; a high
318 concentration of esker ridges within the southern sector of the esker display a spatial correspondence to
319 the fault and associated valley (Fig. 4d). This includes individual ridges in the central sector of the
320 Evishanoran Esker being coincident with faults, where the main esker trends NE-SW (Fig. 2c). Further
321 examples of correspondence between geological faults and eskers are not limited to the Evishanoran
322 Esker: to the west a small series of eskers change orientation to follow a fault which trends NW-SE,
323 highlighted in Figure 2c. These changes occur three times over the ~ 5 km length of this esker.

324 *4.2 Esker Internal Architecture*

325 *4.2.1 Radar facies (RF) description and interpretation*

326 The GPR radar facies from both shielded 160MHz and unshielded 100MHz Rough Terrain antennas
327 were found to be broadly comparable (see below) and are outlined in Table 1. In this section we describe
328 facies characteristics in detail and interpret the depositional environments.

329 *4.2.1 RF1 – Coarse, poorly-bedded deposits*

330 RF1 often constitutes the core of the esker ridge, forming a tabular unit (up to 10 m thick) of
331 discontinuous, chaotic reflectors subparallel to the bed slope. The lower portion of RF1 often contains
332 hyperbola-generating point reflections. This unit is conformably overlain by RF2 or RF3, or truncated
333 by RF4 (Table 1).

334 Chaotic facies have been widely attributed to coarse, poorly-sorted deposits (Burke et al., 2008; Pellicer
335 and Gibson, 2011; Franke *et al.*, 2015; Livingstone et al., 2016; Perkins et al., 2016). This is supported
336 by sediment exposures through RF1, which comprise a variety of massive, coarse, gravelly or diamictic
337 deposits interpreted to have formed by the rapid deposition of hyperconcentrated flows (Fig. 5c; 5d)
338 (Saunderson, 1977; Gorrell and Shaw, 1991; Pellicer and Gibson, 2011; Pellicer et al., 2012;
339 Livingstone et al., 2016; Lang *et al.*, 2017). Previous studies consider point reflections to represent out-
340 of-plane boulder clusters and a coarsening of material within the ridge (Burke, 2010; Burke et al., 2012).
341 Out of plane reflections (sideswipes and hyperbola) are observed to be artefacts of upstanding surface
342 objects such as trees, poles and metal farm gates (Neal, 2004). These are most notable on data from the
343 100MHz unshielded antenna, and thus are disregarded in our interpretations.

344 *4.2.2 RF2 – Horizontally-bedded sands*

345 RF2 generally forms tabular units (~5 m thick) of continuous, subhorizontal reflectors (up to 30 m long)
346 that form parallel to the bed slope (<5° dip from horizontal). It typically forms a central unit in the esker
347 profile, regularly underlain by RF1 and overlain by RF3.

348 Previous studies have attributed similar patterns of subhorizontal reflectors to the vertical accretion of
349 finer material (Perkins et al., 2016). This interpretation is consistent with sediment exposures through

350 RF2 (Fig. 5a), which reveal horizontally-bedded sands and gravels, likely deposited in a lower flow
351 energy environment than RF1 (Banerjee and McDonald, 1975; Burke et al., 2012).

352 4.2.3 RF3 – Delta foresets composed of sands and gravelly sand

353 RF3 forms laterally constrained, wedge-shaped units (2 – 5 m thick) which unconformably overlie the
354 older esker deposits (Table 1). They comprise a series of onlapping, low-angle (4° - 15° from
355 horizontal), N to NE dipping reflections. RF3 is always the topmost unit where identified and therefore
356 represents the final stage of esker building.

357 We interpret the dipping reflectors as foreset beds deposited during lower energy flow conditions
358 compared to RF1 (Fiore et al., 2002; Burke et al., 2008, 2010). Foreset-backset macroforms in eskers
359 are indicative of deposition in a subglacial conduit widening during high-energy flows (Burke *et al.*,
360 2010). As we do not observe any backsets associated with the foreset deposits, deposition is likely not
361 within a subglacial conduit widening. A sediment exposure located NE of a radar survey within a ridge
362 dominated by RF3 (Fig. 9) documents a <1 m thick unit of gravelly-sand, cross-stratified and downflow-
363 dipping deposits (Fig. 5b). These foreset deposits are interpreted to have formed due to a change in
364 hydraulic conditions related to flow expansion (Fiore *et al.*, 2002; Winsemann *et al.*, 2007). We interpret
365 these deposits as either delta foresets deposited as water flowed from a subglacial conduit into a
366 proglacial lake, in some places forming shallow-water mouth-bars (Winsemann *et al.*, 2009; 2018; Lang
367 *et al.*, 2017), or subaqueous fan deposits (Winsemann *et al.*, 2009).

368 4.2.4 RF4 – Concave, erosional trough-fills

369 RF4 is defined by strong, concave-upwards bounding reflectors and subhorizontal to concave internal
370 reflectors (Table 1). The bounding reflectors vary in angle, with the units ranging from narrow, steep-
371 sided basins to broader infills, which may extend for up to 60 m along the esker surface and reach
372 thicknesses of up to 10 m. RF4 truncates underlying facies, displaying an erosional, lower bounding
373 surface. Most frequently, RF4 is located near the surface of the esker, but in places is conformably
374 overlain by RF3. RF4 is interpreted as erosional troughs, formed during the late-stages of esker genesis
375 as water incised into the underlying sediments, and subsequently filled as flow conditions waned
376 (Gorrell and Shaw, 1991; Sambrook-Smith et al., 2006; Perkins et al., 2016).

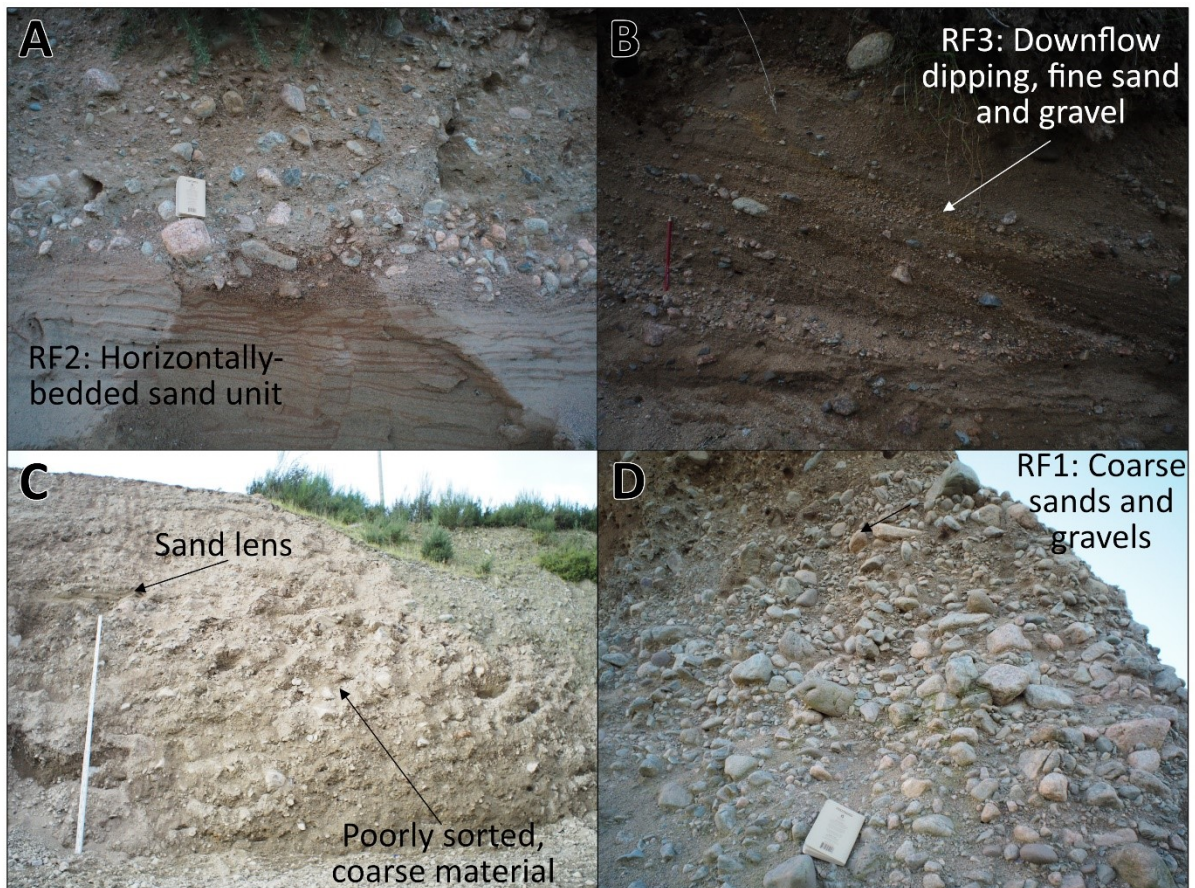
	Southern sector	Central sector	Northern sector
Planform	Complex, multi-ridge	Complex, tributary system	Simple
Average ridge length (m)	357	334	678
Sinuosity	1.17	1.21	1.20
Topographic context	Normal slope through undulating topography	Normal slope through hilly topography	Reverse slope through a uniform valley bottom
Relative relief (m)	~7	~6	~10-15
Total esker length (km)	~6.5 (36 ridges)	~7.4 (39 ridges)	~9.3 (10 ridges)

377 Table 2. The key morphological characteristics of the complex esker system in County Tyrone. The
378 distance along the crestline of each ridge was measured to define the average ridge length. Esker
379 sinuosity was calculated for each individual ridge by dividing the esker ridge length by the straight-line
380 distance from esker initiation to terminus, and is presented as a mean for each sector.

381

382 *4.2.5 RF5 – Post-glacial infill*

383 Present along the flanks in cross-profile surveys of esker ridges, RF5 is separated from the main esker
384 ridge elements by a strong bounding surface, which dips steeply away from the esker (Table 1). The
385 interior of these units is strongly attenuated and characterised by homogenous reflections, which are
386 broadly horizontal. RF5 is interpreted as postglacial infill of the area surrounding the esker ridge. The
387 reflection patterns are consistent with that of peat, which is prevalent across Ireland and confirmed by
388 observations in the field (Jol and Smith, 1991; Pellicer *et al.*, 2012).



389

390 Figure 5. (a) Sediment exposure from the southern-end of the northern sector, consisting of a series of
 391 horizontally stratified sands (RF2), overlain by a poorly sorted sand and gravel unit (54.668°N, -
 392 6.950°E). (b) Sediment exposure within the central, complex esker system, dominated by a series of
 393 downflow-dipping sands and gravelly sands associated with RF3 (54.650°N, -6.953°E). (c) Quarried
 394 section of the single esker ridge system to the north of (a). Facies consist of coarse, diamictic material
 395 with boulders up to 50 cm (54.672°N, -6.941°E). (d) Poorly-sorted sand and gravel units observed
 396 within the northern sector, commonly associated with RF1 (54.668°N, -6.950°E).

397 *4.3 Site architecture*

398 At each site, radar profiles were divided into radar facies according to Table 1 and Section 4.2 above.
 399 Here we describe the architecture of individual esker ridges and outline the processes responsible for
 400 their formation.

401 *4.3.1 Site 1*

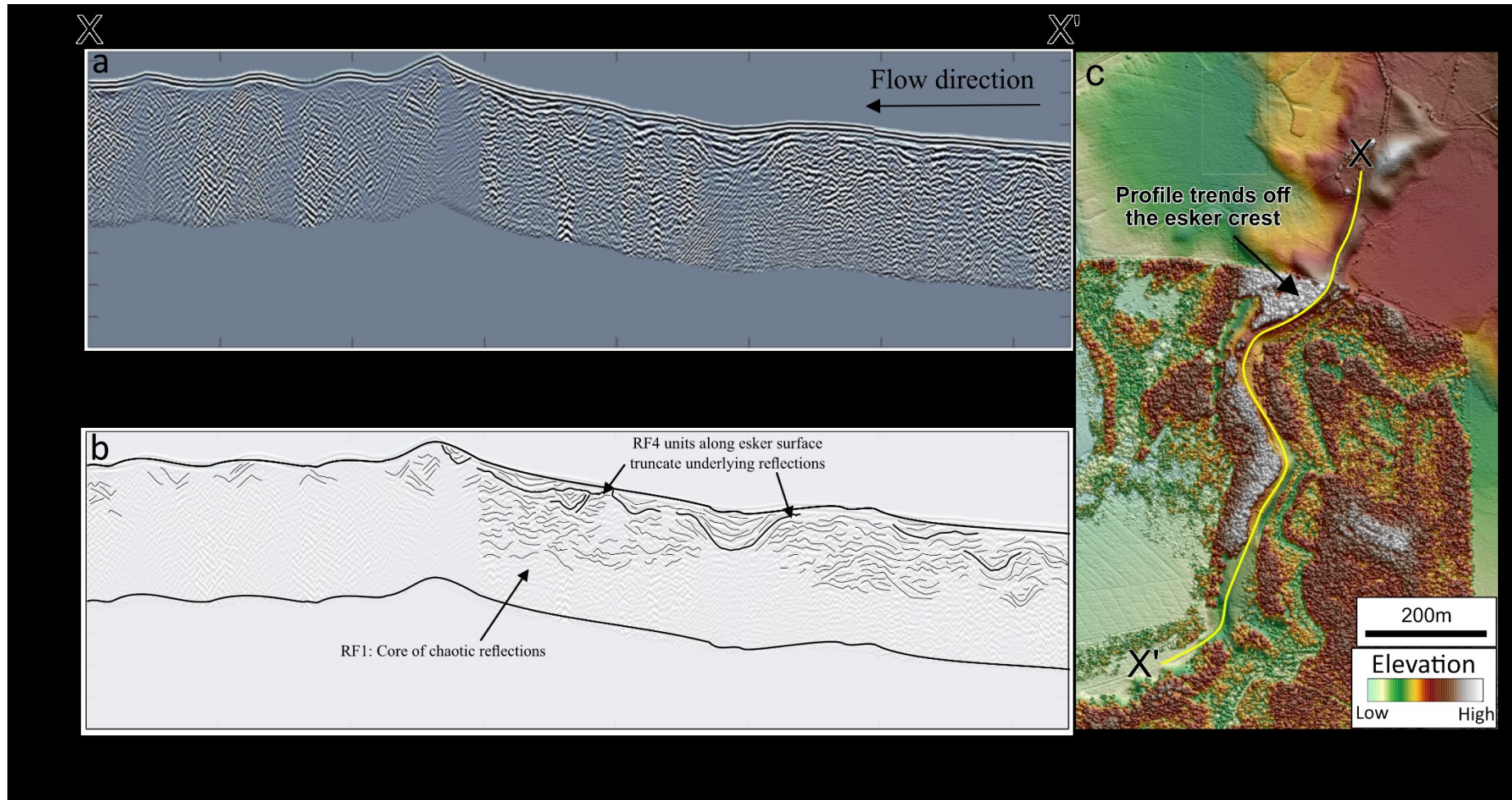
402 Site 1 is a 1.6 km long, broad, round-crested esker ridge at the northern termination of the single ridge
 403 esker system (northern sector). We conducted a 0.9 km, 100 MHz radar survey along a road following
 404 the crest of the esker ridge (Fig. 6). The ridge is situated along a forest-covered valley bottom on a slope
 405 that dips towards the southwest and is significantly wider than southerly ridges within the system (up
 406 to 140 m wide and 16 m high). The esker surface displays minor undulations (<1 m over ~ 90 m).

407 The architecture of the esker ridge is defined by a semi-continuous bounding surface with varying
408 elevation along the upper part of the radar profile (Fig. 6). Below this bounding surface is a core of RF1
409 present along the whole esker profile. The chaotic reflections suggest coarser material with a lack of
410 structure, so are interpreted to have formed by rapid deposition during high flow velocities (Burke *et*
411 *al.*, 2010; Pellicer and Gibson, 2011; Franke *et al.*, 2015; Livingstone *et al.*, 2016). At around 500 m
412 along the profile, side-swipes are observed, likely relating to signal scattering from surface obstacles
413 (Cassidy and Jol, 2009). No lower bounding surface is observed for this unit, but a maximum thickness
414 of 15 m is present at ~ 600 m. Towards the esker surface, the semi-continuous bounding surface defines
415 units of RF4 from 250 m onwards. The concave trough fills (RF4) vary in size, up to ~ 6 m deep and ~
416 80 m wide. At multiple locations the contact with RF4 and underlying reflectors is erosional (Fig. 6).
417 The reflectors observed in these concave infills are less chaotic, which we interpret to have formed as
418 erosional troughs infilled by finer sediment as flow energy waned (Sambrook-Smith *et al.*, 2006; Franke
419 *et al.*, 2015; Table 1). Trough-fill features observed in eskers have previously been interpreted to occur
420 when thermomechanical excavation is outweighed by creep closure, leading to increased flow velocities
421 and the erosion of underlying sediments (Perkins *et al.*, 2016).

422 4.3.2 Site 2

423 Fig. 7 shows a 0.6 km, 160 MHz radar profile taken along the crest of a 1.9 km long, round-crested
424 ridge, near the southern end of the simple esker system (northern sector). Fig. 8 displays a cross-profile
425 (including a short long-profile section of the crestline), taken from just over halfway along the ridge.
426 The topographic context of the system is largely uniform, with the ridge trending up a reverse bed slope
427 along the valley floor. The ridge morphology varies along its length. Undulations (up to 2 m high) are
428 observed to be associated with esker widening, and the ridge generally becomes smaller towards the
429 north (downflow), terminating in a fan-shaped deposit.

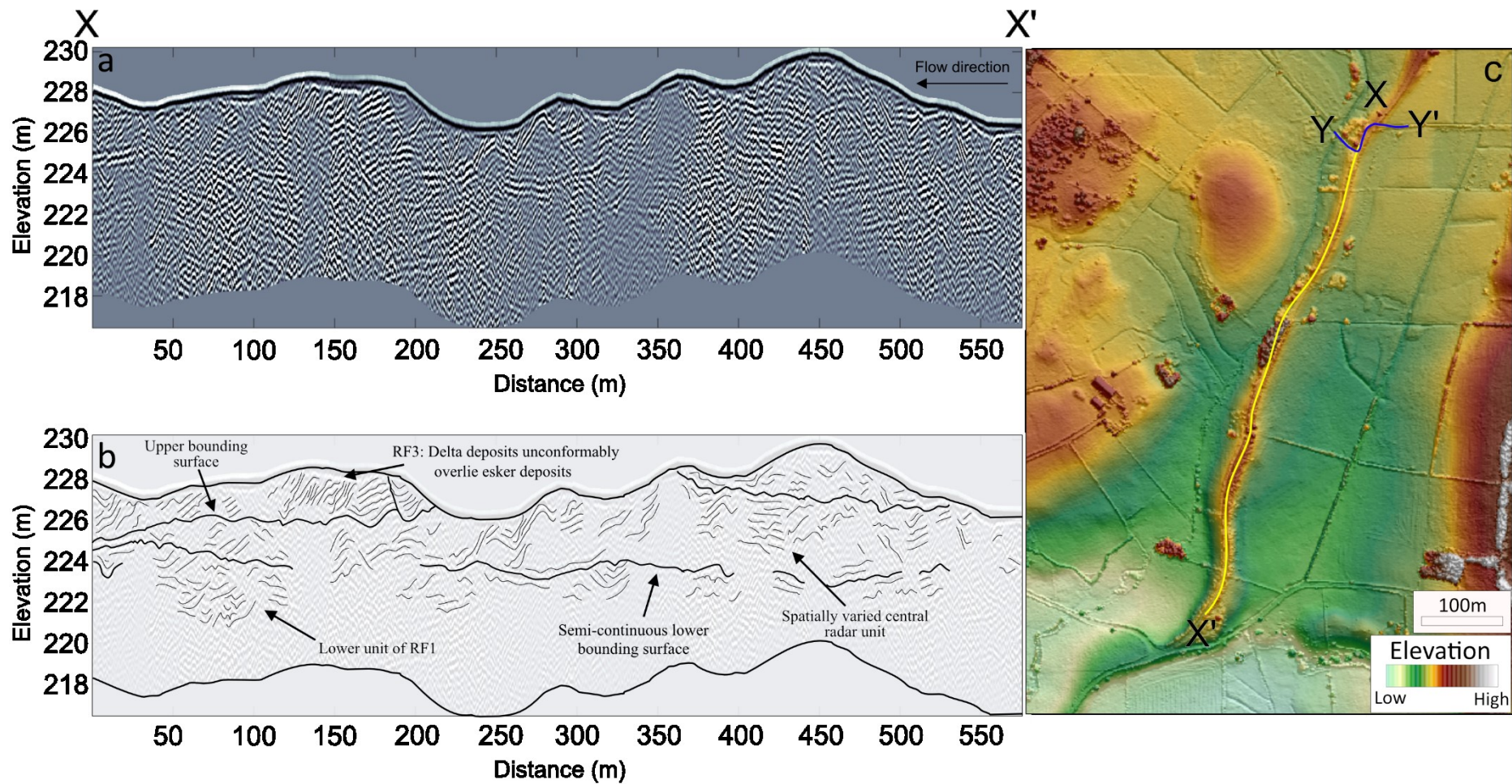
430



431

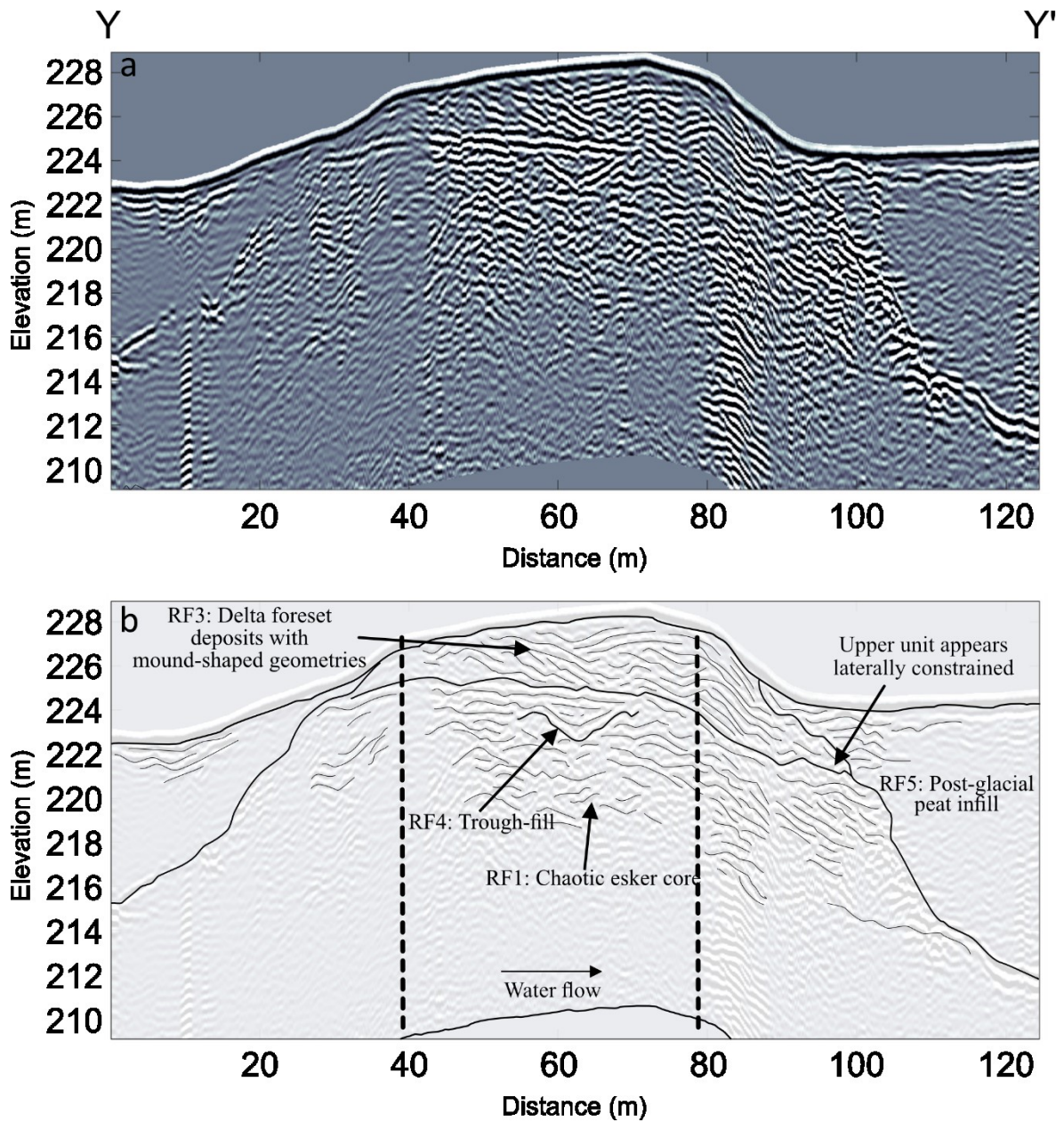
432 Figure 6. (a) 100 MHz long-profile radar survey along the crest of a single ridge esker towards the NE terminus of the County Tyrone Esker, the location of the
 433 survey line is presented in Fig. 2. Ice flow direction is indicated by the black arrow. (b) shows an interpreted radar profile derived through the tracing of key
 434 reflections. (c) Inset figure showing the detailed esker morphology and the location of radar survey (yellow line).

435



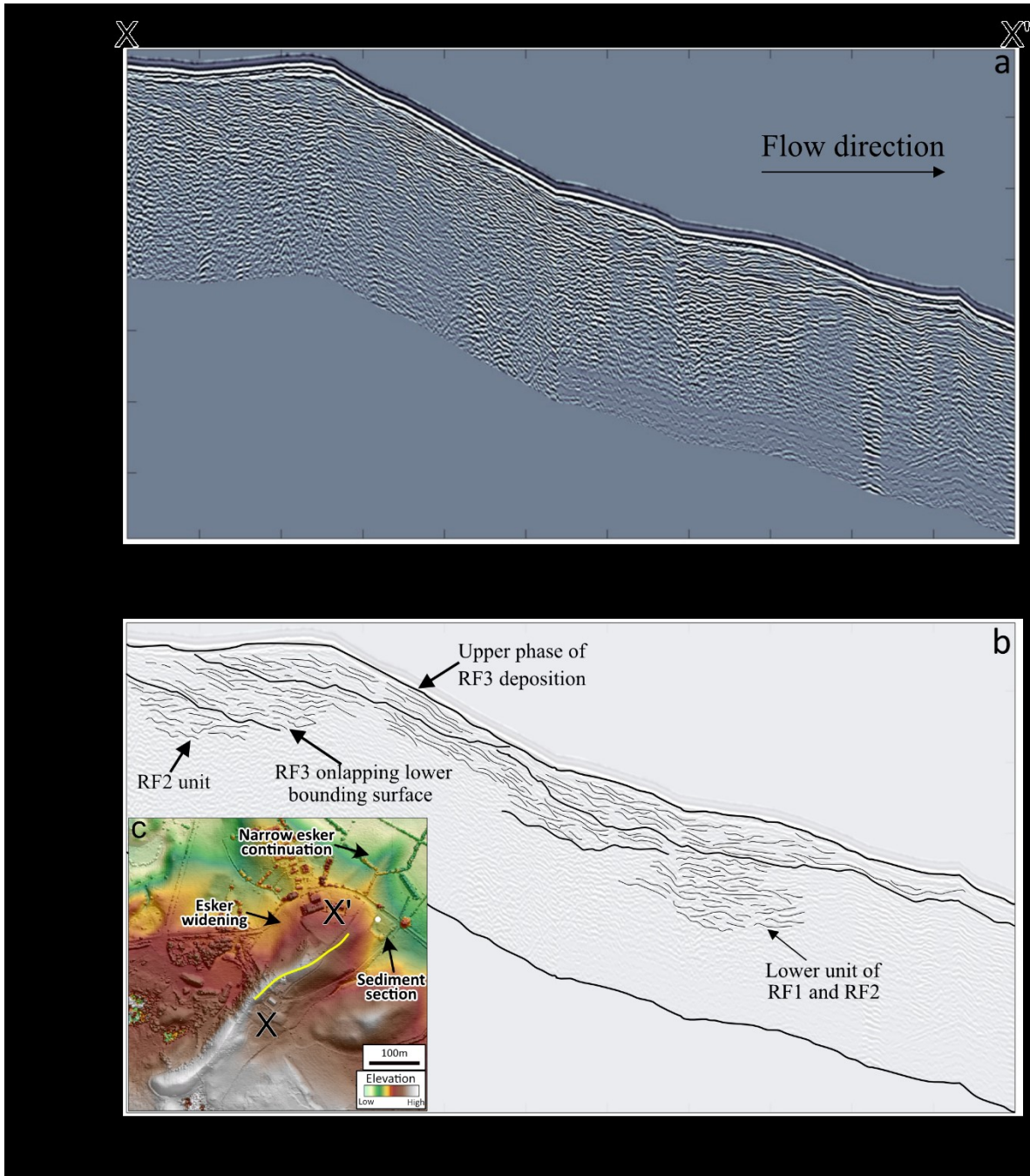
436

437 Figure 7. (a) 160 MHz long-profile radar survey along the crest of a single ridge esker near the initiation of the simple system, the location of the survey line is
 438 presented in Fig. 2. Ice flow direction is indicated by the black arrow. (b) shows an interpreted radar profile derived through the tracing of key reflections. (c)
 439 Inset figure showing the detailed esker morphology and the location of radar surveys for figure 7 (yellow line) and figure 8 (blue line).

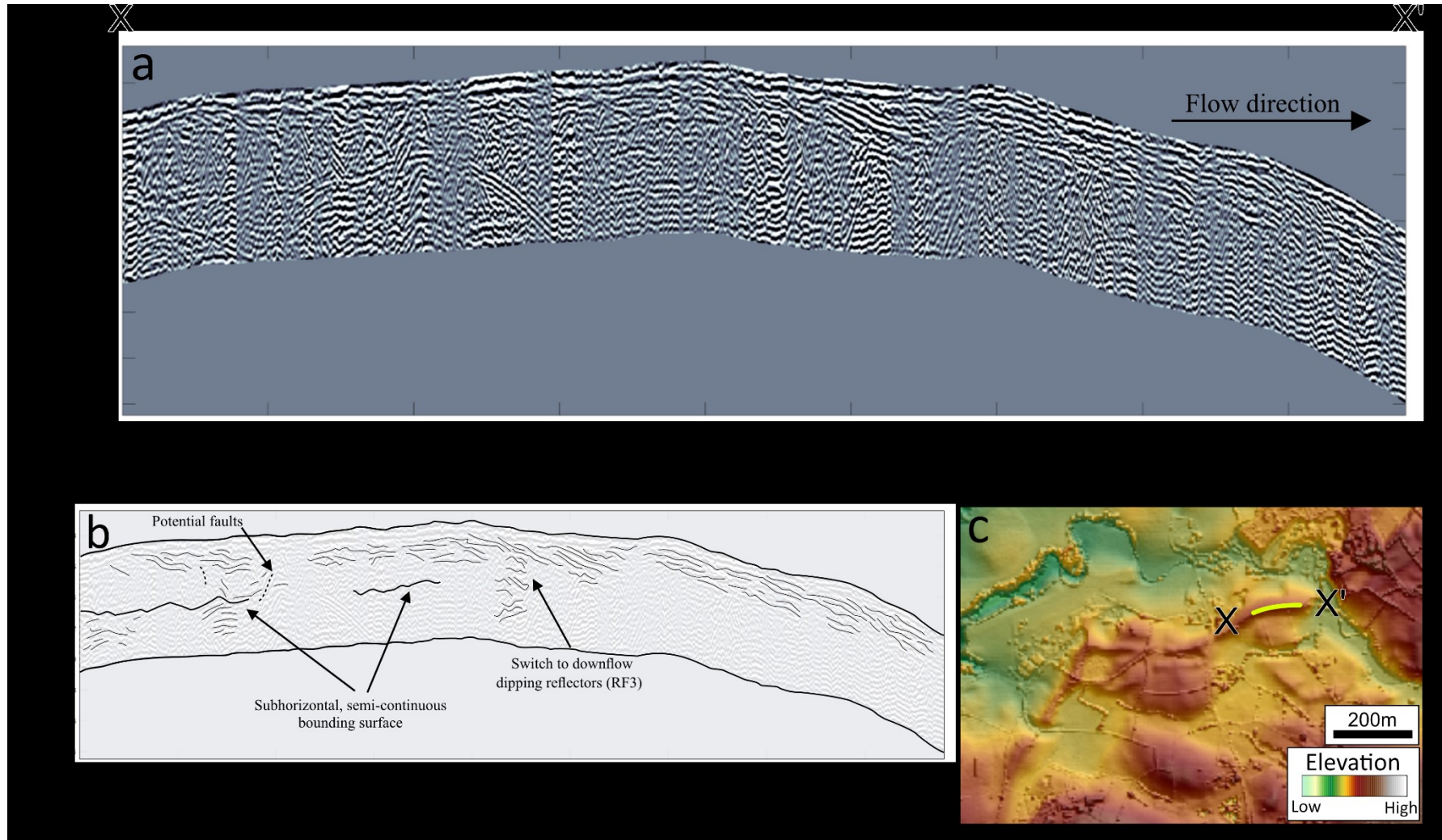


440

441 Figure 8. (a) 160 MHz cross-profile radar survey of a single ridge esker near the initiation of the northern
 442 sector. (b) shows an interpreted radar profile derived through the tracing of key reflections. Vertical
 443 dashed lines indicate the portion of the radar survey which travelled along the esker ridge. The location
 444 of the radar profile is indicated on Fig. 7c by a blue line.



445
 446 Figure 9. (a) 160 MHz radar profile along the crest of an esker within the complex central sector. Ice
 447 flow direction is indicated by the black arrow. (b) shows an interpreted radar profile derived through
 448 the tracing of key reflections. (c) Inset figure showing the detailed esker morphology and the location
 449 of radar survey (yellow line), while the labelled sediment section (white dot) is photographed in Fig.
 450 5b.



451

452 Figure 10. (a) 160 MHz radar profile along the crest of an esker within the southern sector. Ice flow direction is indicated by the black arrow. (b) shows an
 453 interpreted radar profile derived through the tracing of key reflections. (c) Inset figure showing the detailed esker morphology and the location of radar survey
 454 (yellow line).

455 Two strong, horizontal bounding reflectors divide the ridge into three architectural units. These
456 bounding surfaces are discordant with the undulating esker surface. The lowest bounding surface is
457 observed at ~224 m elevation, with the underlying unit comprising a core of RF1 (present along the
458 length of the profile). Variations in thickness (~1 - 4 m) are observed, although no clear esker base is
459 identified. Between 0 - 10 m distance, a single unit of RF4 is present, cutting into RF1 with a depth of
460 ~1 m. This lower radar element relates to the initial stages of esker formation, and indicates high flow
461 energy and deposition of coarse material (Pellicer and Gibson, 2011; Livingstone *et al.*, 2016). Above
462 the bounding surface at ~224m elevation, the radar facies of the central unit varies spatially. Chaotic
463 reflections (RF1) dominate the upflow section from 400 – 550 m distance. Moving downflow, these
464 reflections become more continuous and in places exhibit a downflow dip (RF3; ~ 250m distance). The
465 change to more continuous reflectors indicates the deposition of finer, better sorted material, perhaps
466 due to lower energy flow conditions. Above the upper bounding surface (225 m elevation), a ~2 m
467 thick, tabular unit of RF3 is continuous between 0 – 200 m distance, but absent from 200 – 400 m
468 distance. The presence of coherent downflow dipping reflectors (RF3) indicates a switch to lower flow
469 energy conditions in a progradational depositional environment. Within Fig. 8, RF3 has a convex-up,
470 lenticular reflector pattern. This may represent laterally and vertically stacked delta mouth-bar lobes
471 deposited at the ice sheet margin where water from the subglacial conduit enters a glacial lake
472 (Winsemann *et al.*, 2018). However, we are cautious not to overinterpret this portion of the radar survey
473 due to the non-linear survey route. This unit unconformably overlies the esker core and does not extend
474 over the esker flanks, coinciding with an increase in esker height. This suggests that deposition might
475 have been constrained by ice walls (Fig. 8). Foreset-backset macroforms have been associated with
476 dynamic subglacial conduit enlargements during high flow energy conditions (Fiore *et al.*, 2002; Burke
477 *et al.*, 2010). The absence of backset deposits within this esker suggests another mechanism was
478 responsible for the change to progradational deposition. We suggest the upper unit of RF3 represents
479 deposition of shallow-water mouth-bars at a lake terminating ice sheet margin.

480 Between 400 - 500 m distance, subhorizontal to chaotic reflections (RF1 and RF2) are observed along
481 the esker surface, coincident with an undulation and widening of the esker ridge. Overall, esker
482 architecture records a transition from hyperconcentrated flows during the initial stages, to lower energy
483 flow conditions and the deposition of delta foresets at the ice sheet margin. In cross-profile, up to 8 m
484 of post-glacial peat deposition (RF5) is documented on the esker flanks. This may result in less than
485 50% of the true esker height being observable at the surface (Jol and Smith, 1991; Pellicer *et al.*, 2012).

486 4.3.3 Site 3

487 Fig. 9 presents a 0.2 km, 160 MHz radar profile along the crest of a 0.8 km long round-topped esker
488 ridge, within the complex multi-ridge system (central sector). The ridge is situated in an area of steep,
489 hilly topography. At ~300 m along the esker morphology develops from a narrow ridge (~50 m wide)
490 into a broad, fan-shaped enlargement which is ~130 m wide and ~250 m long, before the ridge
491 terminates in a narrower section (~50 m wide) that is ~200 m long in an open topographic basin that

492 drains to the northwest. The radar profile starts on the summit of a hill at the beginning of the
493 enlargement and then follows the esker crest downslope (Fig 9). Three other ridges are located adjacent
494 to the studied esker, terminating in the same basin. A gravel pit is located at the terminus of the ridge,
495 consisting of a series of sand and gravel foreset units which dip to the northeast (Fig. 5b).

496 Within the lowest radar unit, between 0 – 40 m distance, the sequence is dominated by at least 3 m of
497 coherent horizontal reflections (RF2) indicating vertical accretion of fine material (Burke *et al.*, 2012).
498 Poor radar penetration prevents the identification of the lower bounding surface of this unit. From 120
499 – 170 m along flow, a unit up to 7 m thick, composed of more discontinuous reflections (RF1 and RF2),
500 represents a lateral transition to coarser material lacking structure, interpreted to be deposited
501 subglacially under higher flow energy (Pellicer and Gibson, 2011; Franke *et al.*, 2015; Livingstone *et*
502 *al.*, 2016). The upper section of the radar profiles is dominated by continuous, downflow-dipping
503 parallel reflectors which are convex-up lenticular perpendicular to flow. These units are typically quite
504 thin (up to ~2m) with low dip angles. From 0 – 140 m, there are two units of RF3 along the surface, but
505 140 m onwards is characterised by a single unit of RF3 along the surface. These upper units likely
506 represent a series of delta foresets and cross-stratified sands and gravels, deposited during lower energy
507 flow conditions in a progradational environment (Franke *et al.*, 2015). The thin beds and low dip angle
508 suggest deposition within a shallow water environment (Winsemann *et al.*, 2018). We interpret this
509 sequence of foresets, composed of cross-stratified sands and gravels, as shallow-water delta foresets
510 deposited on top of an esker, as meltwater exits the subglacial conduit at the ice sheet margin
511 (Winsemann *et al.*, 2007). The transition to a broader, fan-shaped morphology of the esker enlargement
512 associated with RF3 supports the interpretation that the delta foresets are superimposed on a core of
513 esker material that was deposited subglacially (Fig. 9).

514 4.3.4 Site 4

515 Fig. 10 shows a 0.18 km long, 160 MHz radar profile along part of the crest of a 0.75 km long round-
516 crested esker within the complex, multi-ridge to anabranching esker system (southern sector). The esker
517 system is situated in an area of complex, hilly topography. The general esker trend is subparallel to a
518 fault-controlled valley, with ridges situated in and around it (Fig. 5d).

519 A single bounding surface is semi-continuous along the radar profile, present from 0 – 70 m distance,
520 at an elevation of ~ 233 m (Fig. 10). Below this bounding surface, a ~2 m thick core unit of chaotic
521 reflections (RF1) is present in sections of the radar profile where penetration was deep enough. These
522 chaotic reflections suggest the presence of coarse material deposited under high energy flow conditions
523 (Pellicer and Gibson, 2011; Livingstone *et al.*, 2016). Above the bounding surface, the radar units (~4
524 m thick) comprise more continuous reflections which are either subhorizontal or downflow dipping
525 (RF2 and RF3). This represents an increase in structure as finer material was deposited during lower
526 energy flow conditions (Franke *et al.*, 2015). The upflow section (0 - 80 m distance) is dominated by

527 RF1 and RF2, while the downflow section (80 m distance onwards) consists of more coherent units of
528 RF3. This transition to fine-grained foresets (RF3) coincides with a change to a downslope trend.

529 **5.0 Discussion**

530 The following section seeks to further our understanding of esker formation based on the sedimentary
531 architecture of a morphologically diverse esker system. First, the broad-scale architecture is considered
532 in order to develop a depositional model of esker formation. Second, local controls on esker formation
533 and morphology are discussed. Finally, we use our findings to reconstruct the ice sheet retreat pattern
534 and retreat rate for the Omagh Basin region.

535 5.1 Esker formation

536 a. A time-transgressive model of esker deposition

537 The Evishanoran Esker has a broadly homogeneous large-scale sedimentary architecture, despite
538 changes in esker morphology and topographic context (Figs. 6-10). GPR surveys reveal two main styles
539 of deposition during esker formation. Initial esker growth involved deposition of coarse gravel or
540 diamict from subglacial hyperconcentrated flows, which may have occurred in a somewhat synchronous
541 manner (Saunderson, 1977; Gorrell and Shaw, 1991; Pellicer and Gibson, 2011). Although, offset ridge
542 relationships and eskers terminating in subaqueous fans or deltas in the northern sector suggest that this
543 deposition likely extended for a maximum of a few kilometres up-ice, rather than tens of kilometres
544 (Fig. 4b). Later stages of esker growth coincide with a transition to well-sorted, deposits as flow energy
545 waned (Franke *et al.*, 2015). The sedimentary structures document a variety of hydrological processes
546 during the final stages of formation (RF2, RF3 and RF4), in contrast to the simple earlier event
547 dominated by hyperconcentrated flows (RF1).

548 As meltwater approaches the ice sheet margin, subglacial conduits experience reduced creep closure
549 (reaching zero at the ice margin: Rothlisberger, 1972). Despite this, thermomechanical excavation
550 continues to enlarge the subglacial conduit, meaning that the subglacial conduit grows towards the ice
551 sheet margin (Drews *et al.*, 2017). This expansion of the subglacial conduit is expected to cause a
552 progressive reduction in flow energy (Hewitt and Creyts, 2019), and thus a reduction of the carrying
553 capacity and the deposition of well-sorted, finer material. Therefore, sedimentation rates are highest at
554 the ice sheet margin (Beaud *et al.*, 2018). This results in an enlargement of the esker profile at or near
555 to former ice margin standstills (Fig. 11a). Additionally, as meltwater exits the subglacial conduit at the
556 ice sheet margin, flow expansion will result in a rapid fall in flow energy and the formation of
557 deltas/outwash fans and foreset deposits (Winsemann *et al.*, 2007). In this situation, the observed
558 vertical upwards-sorting sequence is associated with decreasing flow energy as deposition occurs
559 progressively closer to the ice sheet margin during retreat (Walther, 1894).

560 Esker size, and the thickness of stratigraphic units, is dependent on the duration and rate of deposition.
561 As we described, the deposition rate is likely linked to the proximity of a location to the ice sheet
562 margin, as well as rates of sediment supply. The duration of deposition is related to the rate of ice sheet

563 margin retreat. Rapid margin retreat will reduce the time available for deposition, while a standstill will
564 result in enhanced deposition at and near the ice sheet margin. Therefore, we suggest that enlargements
565 in the esker profile could indicate former ice margin positions. For a stable ice sheet margin position,
566 we would expect a simple esker profile which grows in size towards its terminus. However, variations
567 in the retreat rate during deglaciation will lead to the superimposition of later esker deposits during
568 time-transgressive esker formation (Fig. 11b). We suggest the observed esker enlargements are a form
569 of esker bead deposited time-transgressively at the ice sheet margin (e.g. Livingstone *et al.*, 2020), and
570 superimposed on the core of subglacially deposited coarser material (Fig. 7, 9 and 11).

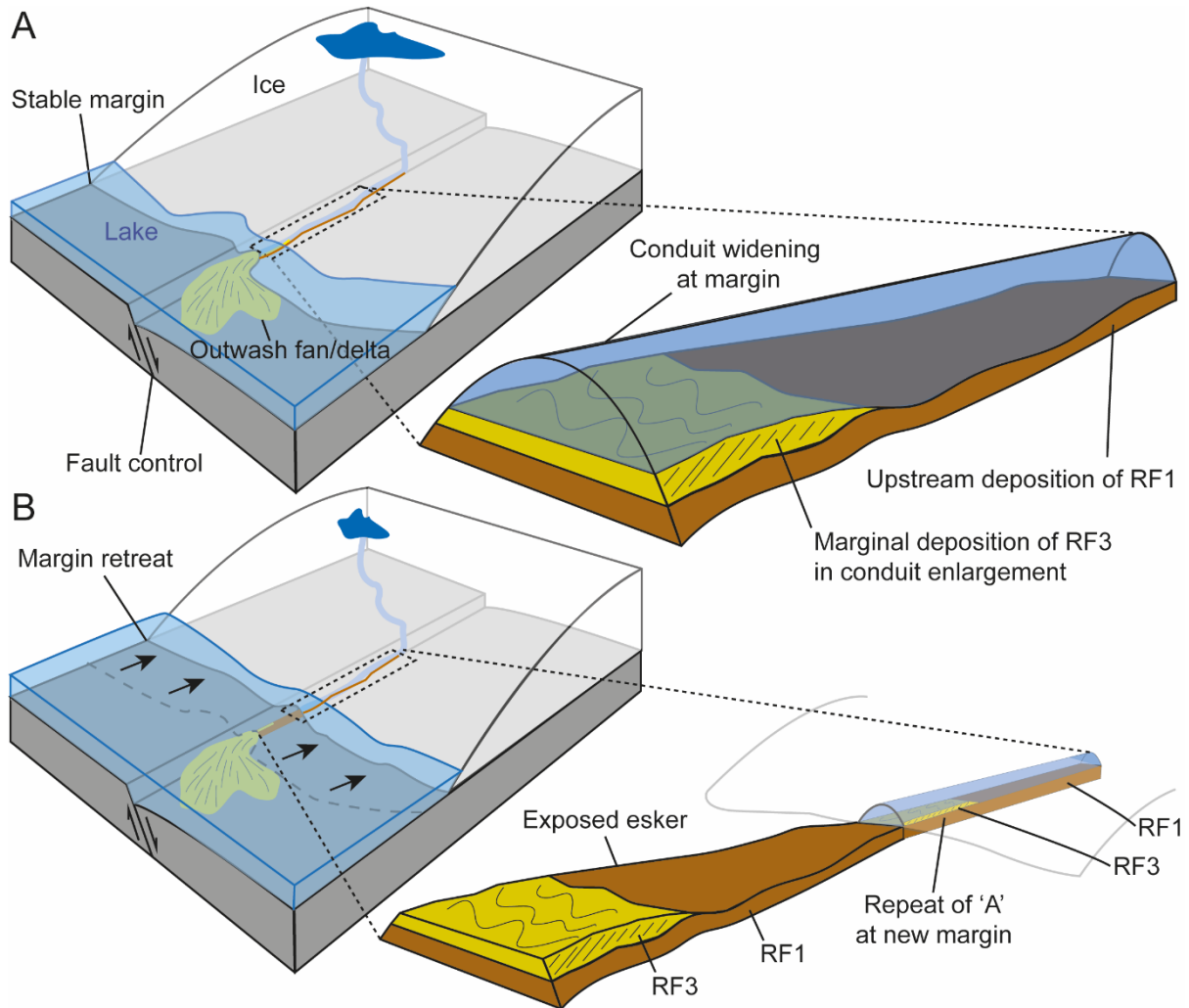
571 Enlargements in eskers or outwash fans/deltas are commonly observed across the Evishanoran Esker.
572 We suggest these enlargements can be used to reconstruct the relative ice sheet margin retreat rate and
573 former ice margin positions. We favour enlargement formation at the ice sheet margin, over the
574 possibility of formation within the subglacial conduits, as we do not observe a backset-foreset
575 macroform diagnostic of this formation (Burke *et al.*, 2015). Caution must be taken when using these
576 to reconstruct the retreat rate, as variations in sediment supply may also influence the development of
577 these enlargements. But, the common co-occurrence of esker enlargements with topographic pinning
578 points (Fig. 4a) or moraines (Fig. 4b) supports an ice marginal origin for esker enlargements.

579 Morphogenetic relationships have been proposed for eskers on the southern Fraser Plateau, British
580 Columbia (Burke *et al.*, 2015; Perkins *et al.*, 2016), while esker complexity has been related to
581 meltwater flow conditions and sediment supply in Svalbard and Iceland (Storrar *et al.*, 2015, 2020). In
582 central Northern Ireland, the relationship between esker morphology and the depositional processes is
583 less clear. At the local scale, undulations and enlargements of the esker profile appear to relate to a
584 time-transgressive depositional model during ice sheet retreat. An esker core is formed by synchronous
585 subglacial deposition, while enlargements are formed by the time-transgressive deposition of sediment
586 at or near to the ice sheet margin (Fig. 11).

587 b. Local controls

588 The morphology of eskers is influenced by the overall drainage characteristics during formation (Burke
589 *et al.*, 2015; Storrar *et al.*, 2015), as well as local factors (Clark and Walder, 1994; Storrar *et al.*, 2014a;
590 Knight, 2019). Beneath the Laurentide Ice Sheet, complex eskers and drainage routeways are more
591 common in areas of greater topographic variability (Storrar *et al.*, 2014a; Lewington *et al.*, 2020). In
592 the Evishanoran Esker, a similar relationship between complex esker morphology and topography is
593 observed. At the large-scale, the complex southern and central esker planforms are associated with a
594 topographic context dominated by high variations in relief, while the simpler northern sector is located
595 on the bottom of a broad valley floor. The distribution of eskers in the central sector clearly illustrates
596 this topographic influence, as eskers are deflected around the ~100m hill (Fig. 4c). We propose that
597 esker complexity in central Northern Ireland is largely controlled by the topographic variability.

598 Undulating topography may cause the subglacial conduit to fragment around obstacles or migrate as ice
 599 thinned (Wright *et al.*, 2008; Storrar *et al.*, 2014b).



600
 601 Fig. 11. A conceptual model of the time-transgressive esker deposition. (a) Delta foresets are deposited
 602 in a proglacial lake at the ice sheet margin due to conduit widening, while coarser material is deposited
 603 up-ice in the subglacial conduit. (b) Ice margin retreat leads to the deposition of foresets on top of the
 604 core of esker material.

605 The complexity of esker systems in areas of high topographic variability reflects a combination of
 606 spatial and temporal changes in the subglacial drainage network. Within the central sector of the
 607 Evishanoran Esker, the cross-cutting esker patterns suggest that the drainage system evolved over time
 608 to create the complex esker network as the drainage pathways migrated during deglaciation (Fig. 4c).
 609 In contrast, the anabranching nature of the southern sector, with no cross-cutting relationships may
 610 instead represent a drainage network which is fragmented by the complex topography (Fig. 4d). This is
 611 supported by the association with a series of meltwater channels cut into, and ascending, the hill to the
 612 south of this sector (Fig. 2b), which may have been active at similar times. Pressurised meltwater eroded
 613 the meltwater channels on the southern slopes of the hill. Reductions in pressure on the downslope trend

614 then led to the deposition of the esker system (Livingstone et al., 2016). It is also possible that increased
615 deposition on the downslope trend may have led to channel clogging and avulsion (Storrar *et al.*, 2015).

616 Substrate characteristics have been hypothesised to influence the formation and distribution of eskers.
617 Eskers are more common on more resistant bedrock (Clark and Walder, 1994), while esker morphology
618 in north-central Ireland is controlled by a variety of substrate factors, including the influence of pre-
619 existing glacial features (Knight, 2019). The transition from sandstone and limestone in the south to the
620 variably metamorphosed crystalline granites and gabbros in the north does not appear to influence esker
621 distribution in the region south of the Sperrin Mountains. This is despite the fundamental differences in
622 bedrock structure at the crystal scale. However, a high level of spatial correspondence between eskers
623 and geological faults is observed (Fig. 2). This correspondence includes eskers in the southern sector
624 running sub-parallel to a large fault-controlled valley, and pronounced changes in the orientation of
625 eskers to trend along faults (Fig. 2). The valley orientation also likely plays a role in controlling the
626 esker distribution. However, esker distribution appears to be fault-controlled across central Northern
627 Ireland, including in locations where there is no clear topographic control. Enhanced groundwater flow
628 along zones of higher transmissivity (e.g. faults) may influence the distribution of the subglacial
629 drainage system (Boulton *et al.*, 2007a; 2007b; 2009). In central Northern Ireland, this relationship
630 appears to strongly control the bedrock transmissivity and configuration of the subglacial drainage
631 network.

632 The morphometry of eskers may relate to a combination of sediment and meltwater supply (Shreve,
633 1985; Storrar *et al.*, 2015), but caution must be taken when using solely geomorphological observations
634 of eskers to investigate the hydrological system of a palaeo-ice sheet. Radar surveys revealed substantial
635 post-glacial peat infilling around eskers, reducing the relative relief of eskers in the northern sector. The
636 relative relief of one esker is 5 m, but with up to 6 m of esker deposits hidden below the surface (Fig.
637 8). Extensive peat deposits have been documented in the Irish Midlands, up to 5.5 m thick (Pellicer and
638 Gibson, 2011; Pellicer *et al.*, 2012), which must be taken into consideration when using esker
639 dimensions to gain an insight into glacial history.

640 5.2 Implications for deglaciation of Northern Ireland

641 Three main ice dispersal centres operated during the deglaciation of the north of Ireland. This includes
642 an upland ice dispersal centre in the Donegal Mountains, and lowland ice domes in the Lough Neagh
643 and Omagh basins (Knight, 1997; Knight and McCabe, 1997; McCarron, 2013). Across this region,
644 meltwater landforms and small moraines record the final retreat pattern of the Irish Ice Sheet. Here we
645 describe the broader retreat patterns of the Irish Ice Sheet, before using the Evishanoran Esker to
646 describe the retreat rate of the Omagh Basin ice.

647 The Donegal Mountains, Lough Neagh and Omagh ice domes were coalescent at the start of
648 deglaciation, indicated by subglacial bedform patterns (Fig. 2a), but became isolated ice domes
649 following ice sheet thinning and saddle collapse (Fig. 2a and 2b). Eskers oriented radially around the

650 Lough Neagh basin record the final retreat pattern inwards. Lough Neagh ice separated from the Lough
651 Erne/Omagh Basin ice dome along an approximately N-S axis located to the south of the eastern Sperrin
652 Mountains (Fig. 2a). In the west, the Lough Erne ice dome separated from ice sourced from the Donegal
653 and Sligo Mountains sometime between 15-16ka, according to the isochrons of Wilson *et al.* (2019).
654 Lateral meltwater channels record the downwasting of ice flowing from Sligo and Donegal into the
655 Lough Erne Basin, recording when summits became ice-free and the separation of these ice dispersal
656 centres (Fig. 2b). The position of these channels suggests Donegal ice flowed into the Lough Erne
657 Basin, indicating that Donegal ice persisted long enough to flow into a mostly deglaciated Lough Erne
658 Basin (Fig. 2b). This is consistent with dating evidence that suggests that the Donegal Mountains held
659 the final remnants of the British-Irish Ice Sheet (Wilson *et al.*, 2019).

660 The relative retreat rate and former ice margin standstills can be identified from the morphology of the
661 Evishanoran Esker and associated landforms. The initial southwards ice margin retreat from the Sperrin
662 Mountains was quite slow across the northern esker sector. We identify at least four former ice margin
663 standstills over the 9.3 km this sector spans, from evidence of five small moraines, two esker
664 enlargements, three delta/outwash fan deposits and sedimentological information (Fig. 2b,c). These
665 former standstill locations are mostly located at topographic pinning points. The retreat rate was more
666 rapid across the central sector. A single moraine and fan-shaped deposit at the northern end of this sector
667 suggest only one standstill across the 7.4 km sector length. The retreat rate across the southern sector
668 may have slowed slightly, as the retreat direction became oriented towards the SW. Geomorphological
669 evidence suggests one or two possible standstills over a distance of 6.5 km. A small moraine at the
670 north-eastern side of the sector suggests a standstill at the start of esker formation in this sector, where
671 a hill (~150m relative relief) may have acted as a pinning point. A small enlargement associated with
672 foreset deposits may have formed under a short-lived standstill in the centre of this sector (Fig. 10).
673 However, the retreat was likely more rapid than in the northern sector due to the relative lack of
674 geomorphological evidence. Continued retreat to the SW of our study area led to the formation of eskers
675 and meltwater channels throughout the Lough Erne Basin and Fintona Hills (Knight, 2003; 2019).

676 **6.0 Conclusions**

677 The Evishanoran Esker was deposited time-transgressively in a subglacial, closed conduit or at the ice
678 sheet margin and records the final stages of ice retreat in this region from the Sperrin Mountains to the
679 south. Esker distribution is a result of the dynamic evolution of the subglacial hydrological system, and
680 does not record an extensive drainage network. Based on our observations, we present a series of key
681 points regarding the deglacial history and broader implications for esker formation:

- 682 1. Deposition of the Evishanoran Esker occurred in two main types of flow event that repeatedly
683 occur during deglaciation. An initial event of semi-synchronous, subglacial deposition formed
684 the esker core. Followed by a second event of time-transgressive deposition at or near the ice
685 sheet margin. This occurs as the subglacial conduit enlarges due to reduced creep closure,
686 causing an increased deposition of sands and gravels. While at the ice sheet margin, flow

687 expansion leads to the deposition of delta foresets composed of gravelly sands. Esker
688 enlargements occur where these time-transgressive deposits are observed, and likely indicate
689 former ice margin positions.

690 2. The internal architecture of eskers is broadly homogenous across all sectors, suggesting that
691 hydrological conditions are largely comparable across the sectors. Variations in esker
692 morphology cannot solely be attributed to variations in drainage characteristics. Instead, we
693 suggest local topographic conditions influence esker complexity.

694 3. Using evidence for former ice margin standstills we reconstruct the variations in the retreat rate
695 across the Evishanoran Esker. Ice margin retreat across the northern sector was slow, with
696 retreat rate increasing during margin retreat across the central and southern sectors.

697 4. Geologic and topographic settings control esker distribution and formation. The close
698 association between the orientation and distribution of eskers and faults suggest that underlying
699 geological structural weaknesses act as a zone of high meltwater transmissivity. The
700 reconstruction of ice dynamics from meltwater features must also consider the influence of
701 local factors on distribution.

702 5. Post-depositional processes can have a significant influence on esker geomorphology. Post-
703 glacial fluvial erosion has previously been invoked to explain the fragmentation of some esker
704 systems. We identify significant post-glacial peat infilling which masks esker dimensions and
705 poses a problem for esker studies that rely solely on remote sensing morphometric analysis.

706

707 **Acknowledgements:**

708 We thank Mike Langton of GuideLineGeo (MALA) for the loan of radar equipment and advice. Digital
709 resources were made available under MOU205, courtesy of Land and Property Services, Northern
710 Ireland, supplied to Queen's University, Belfast. This study would also not be possible without the
711 generous access to land granted by multiple landowners in Northern Ireland. We kindly thank two
712 anonymous reviewers for their comments on this manuscript.

713

714 **Funding sources:**

715 This research did not receive any specific grant from funding agencies in the public, commercial, or
716 not-for-profit sectors.

717

718 **References:**

719 Alley, R.B., Blankenship, D.D., Bentley, C.R. and Rooney, S.T. (1986) Deformation of till beneath
720 ice stream B, West Antarctica. *Nature*, 322, 57-59.

- 721 Aylsworth, J.M. and Shilts, W.W. (1989) Bedforms of the Keewatin ice sheet, Canada. *Sedimentary*
722 *Geology*, 62(2-4): 407-428
- 723 Banerjee, I. and McDonald, B.C. (1975) Nature of esker sedimentation, in Jopling, A. V., and
724 McDonald, B. C., eds., *Glaciofluvial and glaciolacustrine sedimentation*: Society of
725 Economic Paleontologists and Mineralogists Special Publication No. 23: 132-154.
- 726 Bartholomew, I., Nienow, P., Mair, D., Hubbard, A., King, M.A. and Sole, A. (2010). Seasonal
727 evolution of subglacial drainage and acceleration in a Greenland outlet glacier. *Nature*
728 *Geoscience*, 3(6), 408-411.
- 729 Beaud, F., Flowers, G.E. and Venditti, J.G. (2018) Modeling Sediment Transport in Ice-Walled
730 Subglacial Channels and Its Implications for Esker Formation and Proglacial Sediment
731 Yields. *Journal of Geophysical Research: Earth Surface*, 123(12): 3206-3227
- 732 Bell, R.E., Studinger, M., Shuman, C.A., Fahnestock, M.A. and Joughin, I. (2007). Large subglacial
733 lakes in East Antarctica at the onset of fast-flowing ice streams. *Nature*, 445(7130), 904-
734 907.
- 735 Boulton, G.S., Hagdorn, M., Maillot, P.B. and Zatsepin, S. (2009) Drainage beneath ice sheets:
736 groundwater–channel coupling, and the origin of esker systems from former ice
737 sheets. *Quaternary Science Reviews*, 28(7-8), 621-638
- 738 Boulton, G.S., Lunn, R., Vidstrand, P. and Zatsepin, S. (2007b) Subglacial drainage by
739 groundwater–channel coupling, and the origin of esker systems: part II—theory and
740 simulation of a modern system. *Quaternary Science Reviews*, 26(7-8), 1091-1105
- 741 Boulton, G.S., Lunn, R., Vidstrand, P. and Zatsepin, S., (2007a) Subglacial drainage by
742 groundwater-channel coupling, and the origin of esker systems: part 1—glaciological
743 observations. *Quaternary Science Reviews*, 26(7-8), 1067-1090
- 744 Bradwell, T., Stoker, M.S., Golledge, N.R., Wilson, C.K., Merritt, J.W., Long, D., Everest, J.D.,
745 Hestvik, O.B., Stevenson, A.G., Hubbard, A.L. and Finlayson, A.G. (2008) The northern
746 sector of the last British Ice Sheet: maximum extent and demise. *Earth-Science*
747 *Reviews*, 88(3-4): 207-226
- 748 Brennand, T. A. (1994). Macroforms, large bedforms and rhythmic sedimentary sequences in
749 subglacial eskers, south-central Ontario: implications for esker genesis and meltwater
750 regime. *Sedimentary Geology*, 91(1–4), 9–55. [https://doi.org/10.1016/0037-0738\(94\)90122-](https://doi.org/10.1016/0037-0738(94)90122-8)
751 [8](https://doi.org/10.1016/0037-0738(94)90122-8)

- 752 Brennand, T.A. (2000) Deglacial meltwater drainage and glaciodynamics: inferences from
753 Laurentide eskers, Canada. *Geomorphology*, 32(3-4): 263-293
- 754 Budd, W.F., Keage, P.L. and Blundy, N.A (1979). Empirical studies of ice sliding. *Journal of*
755 *Glaciology*, 23, 157-170.
- 756 Burke, M. J., Brennand, T. A., & Sjogren, D. B. (2015). The role of sediment supply in esker
757 formation and ice tunnel evolution. *Quaternary Science Reviews*, 115, 50–77.
758 <https://doi.org/10.1016/j.quascirev.2015.02.017>
- 759 Burke, M. J., Woodward, J., Russell, A. J., Fleisher, P. J., & Bailey, P. K. (2008). Controls on the
760 sedimentary architecture of a single event englacial esker: Skeiðarárjökull, Iceland.
761 *Quaternary Science Reviews*, 27(19–20): 1829–1847.
762 <https://doi.org/10.1016/j.quascirev.2008.06.012>
- 763 Burke, M. J., Woodward, J., Russell, A. J., Fleisher, P. J., & Bailey, P. K. (2010). The sedimentary
764 architecture of outburst flood eskers: A comparison of ground-penetrating radar data from
765 Bering Glacier, Alaska and Skeiðarárjökull, Iceland. *Bulletin of the Geological Society of*
766 *America*, 122(9–10): 1637–1645. <https://doi.org/10.1130/B30008.1>
- 767 Burke, M.J., Brennand, T.A. and Perkins, A.J. (2012) Transient subglacial hydrology of a thin ice
768 sheet: insights from the Chasm esker, British Columbia, Canada. *Quaternary Science*
769 *Reviews*, 58: 30-55.
- 770 Callard, S.L., Cofaigh, C.Ó., Benetti, S., Chiverrell, R.C., Van Landeghem, K.J., Saher, M.H.,
771 Livingstone, S.J., Clark, C.D., Small, D., Fabel, D. and Moreton, S.G. (2020) Oscillating
772 retreat of the last British-Irish Ice Sheet on the continental shelf offshore Galway Bay,
773 western Ireland. *Marine Geology*, 420: 106087.
- 774 Cassidy, N.J. and Jol, H.M. (2009) Ground penetrating radar data processing, modelling and
775 analysis. *Ground penetrating radar: theory and applications*: 141-176
- 776 Charlesworth, J.K. (1926) The Evishnoran “Esker”, Tyrone. *Geological Magazine*, 63(5), 223-225.
777 doi:10.1017/S0016756800084156
- 778 Charlesworth, J.K. (1924). The glacial geology of the north-west of Ireland. *Proceedings of the*
779 *Royal Irish Academy*, 36b: 174-314
- 780 Chew, D.M., Flowerdew, M.J., Page, L.M., Crowley, Q.G., Daly, J.S., Cooper, M. and Whitehouse,
781 M.J. (2008) The tectonothermal evolution and provenance of the Tyrone Central Inlier,

- 782 Ireland: Grampian imbrication of an outboard Laurentian microcontinent?. *Journal of the*
783 *Geological Society*, 165(3): 675-685
- 784 Chiverrell, R.C., Thomas, G.S.P., Burke, M., Medialdea, A., Smedley, R., Bateman, M., Clark, C.,
785 Duller, G.A., Fabel, D., Jenkins, G. and Ou, X. (2020) The evolution of the terrestrial-
786 terminating Irish Sea glacier during the last glaciation. *Journal of Quaternary Science*,
787 doi:10.1002/jqs.3229
- 788 Clark, C.D. and Meehan, R.T. (2001) Subglacial bedform geomorphology of the Irish Ice Sheet
789 reveals major configuration changes during growth and decay. *Journal of Quaternary*
790 *Science: Published for the Quaternary Research Association*, 16(5): 483-496
- 791 Clark, C.D., Ely, J.C., Greenwood, S.L., Hughes, A.L., Meehan, R., Barr, I.D., Bateman, M.D.,
792 Bradwell, T., Doole, J., Evans, D.J. and Jordan, C.J. (2018) BRITICE Glacial Map, version
793 2: a map and GIS database of glacial landforms of the last British–Irish Ice
794 Sheet. *Boreas*, 47(1): 11
- 795 Clark, C.D., Hughes, A.L., Greenwood, S.L., Jordan, C. and Sejrup, H.P. (2012) Pattern and timing
796 of retreat of the last British-Irish Ice Sheet. *Quaternary Science Reviews*, 44: 112-146
- 797 Clark, P. U., & Walder, J. S. (1994). Subglacial drainage, eskers, and deforming beds beneath the
798 Laurentide and Eurasian ice sheets. *Geological Society of America Bulletin*, 106(2), 304–
799 314. [https://doi.org/10.1130/0016-7606\(1994\)106<0304:SDEADB>2.3.CO;2](https://doi.org/10.1130/0016-7606(1994)106<0304:SDEADB>2.3.CO;2)
- 800 Colhoun, A. (1971) The glacial stratigraphy of the Sperrin Mountains and its relation to the glacial
801 stratigraphy of north-west Ireland. *Proceedings of the Royal Irish Academy* 71B: 37–52
- 802 Colhoun, E.A. (1970). On the nature of the glaciations and final deglaciation of the Sperrin
803 Mountains and adjacent areas in the north of Ireland. *Irish Geography*, 6(2), 162-185.
- 804 Cummings, D.I., Kjarsgaard, B.A., Russell, H.A. and Sharpe, D.R. (2011) Eskers as mineral
805 exploration tools. *Earth-science reviews*, 109(1-2): 32-43
- 806 Dardis, G.F. (1986) Late Pleistocene glacial lakes in south-central Ulster, Northern Ireland. *Irish*
807 *journal of earth sciences*: 133-144
- 808 Davison, B.J., Sole, A.J., Livingstone, S.J., Cowton, T.R. and Nienow, P.W. (2019) The influence of
809 hydrology on the dynamics of land-terminating sectors of the Greenland Ice Sheet. *Frontiers*
810 *in Earth Science*, 7.

- 811 Delaney, C. (2001a) Esker formation and the nature of deglaciation: the Ballymahon esker, Central
812 Ireland. *North West Geography*, 1(2): 23-33
- 813 Delaney, C. (2001b) Morphology and sedimentology of the Rooskagh esker, Co. Roscommon. *Irish*
814 *Journal of Earth Sciences*: 5-22
- 815 Delaney, C. (2002) Sedimentology of a glaciofluvial landsystem, Lough Ree area, Central Ireland:
816 implications for ice margin characteristics during Devensian deglaciation. *Sedimentary*
817 *Geology*, 149(1-3): 111-126
- 818 Delaney, C.A., McCarron, S. and Davis, S. (2018). Irish Ice Sheet dynamics during deglaciation of
819 the central Irish Midlands: Evidence of ice streaming and surging from airborne LiDAR.
820 *Geomorphology*, 306, 235-253.
- 821 Drews, R., Pattyn, F., Hewitt, I.J., Ng, F.S.L., Berger, S., Matsuoka, K., Helm, V., Bergeot, N.,
822 Favier, L. and Neckel, N. (2017) Actively evolving subglacial conduits and eskers initiate
823 ice shelf channels at an Antarctic grounding line. *Nature communications*, 8: 15228
- 824 Dyke, A. and Prest, V. (1987) Late Wisconsinan and Holocene history of the Laurentide ice
825 sheet. *Géographie physique et Quaternaire*, 41(2): 237-263.
- 826 Evans, D. J. A., & Benn, D. I. (2004) A practical guide to the study of glacial sediments. Edward
827 Arnold, London.
- 828 Fiore, J., Pugin, A. and Beres, M. (2002) Sedimentological and GPR studies of subglacial deposits
829 in the Joux Valley (Vaud, Switzerland): backset accretion in an esker followed by an erosive
830 jökulhlaup. *Géographie physique et Quaternaire*, 56(1): 19-32
- 831 Fitzsimons, S.J. (1991) Supraglacial eskers in Antarctica. *Geomorphology*, 4(3-4): 293-299
- 832 Flint, R.F. (1930) The Origin of the Irish" Eskers". *Geographical Review*, 20(4): 615-630
- 833 Franke, D., Hornung, J. and Hinderer, M. (2015) A combined study of radar facies, lithofacies and
834 three-dimensional architecture of an alpine alluvial fan (Illgraben fan,
835 Switzerland). *Sedimentology*, 62(1): 57-86
- 836 Gawthorpe, R.L., Collier, R.L., Alexander, J., Bridge, J.S. and Leeder, M.R. (1993) Ground
837 penetrating radar: application to sandbody geometry and heterogeneity studies. *Geological*
838 *Society, London, Special Publications*, 73(1): 421-432

- 839 Geological Survey Northern Ireland (2016) Digital Geological Map of Northern Ireland – 10k. 10k
840 geology reproduced with the permission of the Geological Survey of Northern Ireland.
841 Crown Copyright 2018.
- 842 Gorrell, G. and Shaw, J. (1991) Deposition in an esker, bead and fan complex, Lanark, Ontario,
843 Canada. *Sedimentary Geology*, 72(3-4): 285-314
- 844 Greenwood, S. L., & Clark, C. D. (2009a). Reconstructing the last Irish Ice Sheet 1: changing flow
845 geometries and ice flow dynamics deciphered from the glacial landform record. *Quaternary*
846 *Science Reviews*, 28(27–28), 3085–3100. <https://doi.org/10.1016/j.quascirev.2009.09.008>
- 847 Greenwood, S. L., & Clark, C. D. (2009b). Reconstructing the last Irish Ice Sheet 2: a
848 geomorphologically-driven model of ice sheet growth, retreat and dynamics. *Quaternary*
849 *Science Reviews*, 28(27–28), 3101–3123. <https://doi.org/10.1016/j.quascirev.2009.09.014>
- 850 Greenwood, S.L., Clark, C.D. and Hughes, A.L. (2007) Formalising an inversion methodology for
851 reconstructing ice-sheet retreat patterns from meltwater channels: application to the British
852 Ice Sheet. *Journal of Quaternary Science: Published for the Quaternary Research*
853 *Association*, 22(6): 637-645
- 854 Greenwood, S.L., Clason, C.C., Helanow, C. and Margold, M. (2016) Theoretical, contemporary
855 observational and palaeo-perspectives on ice sheet hydrology: processes and
856 products. *Earth-Science Reviews*, 155: 1-27
- 857 Gregory, J.W. (1912) The relations of kames and eskers. *The Geographical Journal*, 40(2): 169-175.
- 858 Gregory, J.W. (1921) IV.—The Irish eskers. *Phil. Trans. R. Soc. Lond. B*, 210(372-381): 115-151.
- 859 Gregory, J.W. (1925) The Evishanoran Esker, 1 Tyrone. *Geological Magazine*, 62(10): 451-458.
- 860 Gregory, J.W. (1926) The Evishnoran “Esker”. *Geological Magazine*, 62(7): 336-336.
861 doi:10.1017/S0016756800084557
- 862 Gustavson, T.C. and Boothroyd, J.C. (1987) A depositional model for outwash, sediment sources,
863 and hydrologic characteristics, Malaspina Glacier, Alaska: A modern analog of the
864 southeastern margin of the Laurentide Ice Sheet. *Geological Society of America*
865 *Bulletin*, 99(2): 187-200.
- 866 Hebrand, M. and Åmark, M. (1989) Esker formation and glacier dynamics in eastern Skane and
867 adjacent areas, southern Sweden. *Boreas*, 18(1): 67-81.

- 868 Hewitt, I.J. and Creyts, T.T. (2019) A model for the formation of eskers. *Geophysical Research*
869 *Letters*, 46(12), pp.6673-6680.
- 870 Hinch, J. (1921) The eskers of Ireland. *The Irish Naturalist*, 30(12): 137-142
- 871 Hubbard, B. & Nienow, P. (1997) Alpine subglacial hydrology. *Quaternary Science Reviews*, 16,
872 939-955.
- 873 Iken, A., Bindschadler, R.A. (1986) Combined measurements of subglacial water pressure and
874 surface velocity of Findelengletscher, Switzerland: conclusions about drainage system and
875 sliding mechanism. *Journal of Glaciology*, 32(110): 101-119.
- 876 Jol, H.M. and Smith, D.G. (1991) Ground penetrating radar of northern lacustrine deltas. *Canadian*
877 *Journal of Earth Sciences*, 28(12): 1939-1947
- 878 Knight, J. (1997). Morphological and morphometric analysis of drumlin bedforms in the Omagh
879 Basin, north central Ireland. *Geografiska Annaler*, 79A: 255-266.
- 880 Knight, J. (1999). Geological evidence for neotectonic activity during deglaciation of the southern
881 Sperrin Mountains, Northern Ireland. *Journal of Quaternary Science*, 14(1): 45-57.
- 882 Knight, J. (2002). Bedform patterns, subglacial meltwater events, and Late Devensian ice sheet
883 dynamics in north-central Ireland. *Global and Planetary Change*, 35(3-4): 237-253.
- 884 Knight, J. (2003) Geomorphic evidence for patterns of late Midlandian ice advance and retreat in the
885 Omagh Basin. *Irish Geography*, 36(1): 1-22
- 886 Knight, J. (2006) Geomorphic evidence for active and inactive phases of Late Devensian ice in
887 north-central Ireland. *Geomorphology*, 75(1-2): 4-19
- 888 Knight, J. (2019) The geomorphology and sedimentology of eskers in north-Central
889 Ireland. *Sedimentary Geology*, 382: 1-24.
- 890 Knight, J. and McCabe, A.M. (1997) Identification and significance of ice-flow-transverse
891 subglacial ridges (Rogen moraines) in northern central Ireland. *Journal of Quaternary*
892 *Science*, 12(6): 519-524
- 893 Knight, J., Coxon, P., McCabe, A.M. and McCarron, S.G. (2004) Pleistocene glaciations in Ireland.
894 In *Developments in Quaternary Sciences*, 2: 183 – 191. Elsevier.

- 895 Lang, J., Sievers, J., Loewer, M., Igel, J. and Winsemann, J. (2017) 3D architecture of cyclic-step
896 and antidune deposits in glacial subaqueous fan and delta settings: Integrating outcrop
897 and ground-penetrating radar data. *Sedimentary Geology*, 362: 83-100
- 898 Lewington, E.L., Livingstone, S.J., Clark, C.D., Sole, A.J. and Storrar, R.D. (2020) A model for
899 interaction between conduits and surrounding hydraulically connected distributed drainage
900 based on geomorphological evidence from Keewatin, Canada. *The Cryosphere*, 14(9): 2949-
901 2976.
- 902 Livingstone, S. J., Utting, D. J., Ruffell, A., Clark, C. D., Pawley, S., Atkinson, N., & Fowler, A. C.
903 (2016). Discovery of relict subglacial lakes and their geometry and mechanism of drainage.
904 *Nature Communications*, 7. <https://doi.org/10.1038/ncomms11767>
- 905 Livingstone, S.J., Lewington, E.L., Clark, C.D., Storrar, R.D., Sole, A.J., McMartin, I., Dewald, N.
906 and Ng, F. (2020) A quasi-annual record of time-transgressive esker formation: implications
907 for ice-sheet reconstruction and subglacial hydrology. *The Cryosphere*, 14(6): 1989-2004
- 908 Livingstone, S.J., Storrar, R.D., Hillier, J.K., Stokes, C.R., Clark, C.D. and Tarasov, L. (2015) An
909 ice-sheet scale comparison of eskers with modelled subglacial drainage
910 routes. *Geomorphology*, 246: 104-112
- 911 Mäkinen, J. (2003) Time-transgressive deposits of repeated depositional sequences within
912 interlobate glaciofluvial (esker) sediments in Köyliö, SW Finland. *Sedimentology*, 50(2):
913 327-360
- 914 Margold, M., Jansson, K.N., Kleman, J., Stroeven, A.P. and Clague, J.J. (2013) Retreat pattern of
915 the Cordilleran Ice Sheet in central British Columbia at the end of the last glaciation
916 reconstructed from glacial meltwater landforms. *Boreas*, 42(4): 830-847
- 917 McCarron, S. (2013) Deglaciation of the Dungiven Basin, North-West Ireland. *Irish Journal of*
918 *Earth Sciences*, 31: 43-71
- 919 Miall, A.D. (1985) Architectural-element analysis: a new method of facies analysis applied to fluvial
920 deposits. *Earth Sci. Rev.*, 22: 261–308
- 921 Neal, A. (2004) Ground-penetrating radar and its use in sedimentology: principles, problems and
922 progress. *Earth-science reviews*, 66(3-4): 261-330

- 923 Ó Cofaigh, C., Evans, D.J.A. (2007) Radiocarbon constraints on the age of the maximum advance of
924 the British-Irish Ice Sheet in the Celtic Sea. *Quaternary Science Reviews* 26 (9–10), 1197–
925 1203
- 926 Ó Cofaigh, C., Weilbach, K., Lloyd, J.M., Benetti, S., Callard, S.L., Purcell, C., Chiverrell, R.C.,
927 Dunlop, P., Saher, M., Livingstone, S.J. and Van Landeghem, K.J. (2019) Early deglaciation
928 of the British-Irish Ice Sheet on the Atlantic shelf northwest of Ireland driven by
929 glacioisostatic depression and high relative sea level. *Quaternary Science Reviews*, 208: 76-
930 96
- 931 Pellicer, X. M., & Gibson, P. (2011). Electrical resistivity and Ground Penetrating Radar for the
932 characterisation of the internal architecture of Quaternary sediments in the Midlands of
933 Ireland. *Journal of Applied Geophysics*, 75(4), 638–647.
934 <https://doi.org/10.1016/j.jappgeo.2011.09.019>
- 935 Pellicer, X. M., Warren, W. P., Gibson, P., & Linares, R. (2012). Construction of an evolutionary
936 deglaciation model for the Irish midlands based on the integration of morphostratigraphic
937 and geophysical data analyses. *Journal of Quaternary Science*, 27(8), 807–818.
938 <https://doi.org/10.1002/jqs.2570>
- 939 Perkins, A. J., Brennand, T. A., & Burke, M. J. (2016). Towards a morphogenetic classification of
940 eskers: Implications for modelling ice sheet hydrology. *Quaternary Science Reviews*, 134:
941 19–38. <https://doi.org/10.1016/j.quascirev.2015.12.015>
- 942 Perkins, A.J., Brennand, T.A. and Burke, M.J. (2013) Genesis of an esker-like ridge over the
943 southern Fraser Plateau, British Columbia: Implications for paleo-ice sheet reconstruction
944 based on geomorphic inversion. *Geomorphology*, 190: 27-39
- 945 Price, R.J. (1969) Moraines, sandar, kames and eskers near Breidamerkurjökull,
946 Iceland. *Transactions of the Institute of British Geographers*: 17-43
- 947 Roberts, M.C., Niller, H.P. and Helmstetter, N. (2003) Sedimentary architecture and radar facies of a
948 fan delta, Cypress Creek, West Vancouver, British Columbia. *Geological Society, London,*
949 *Special Publications*, 211(1): 111-126
- 950 Röthlisberger, H. (1972) Water pressure in intra-and subglacial channels. *Journal of*
951 *Glaciology*, 11(62): 177-203

- 952 Russell, A.J., Knudsen, O., Fay, H., Marren, P.M., Heinz, J. and Tronicke, J. (2001) Morphology
953 and sedimentology of a giant supraglacial, ice-walled, jökulhlaup channel, Skeiðarárjökull,
954 Iceland: implications for esker genesis. *Global and Planetary Change*, 28(1-4): 193-216
- 955 Sambrook-Smith, G.H., Ashworth, P.J., Best, J.L., Woodward, J. and Simpson, C.J. (2006) The
956 sedimentology and alluvial architecture of the sandy braided South Saskatchewan River,
957 Canada. *Sedimentology*, 53(2): 413-434
- 958 Saunderson, H.C. (1977) The sliding bed facies in esker sands and gravels: a criterion for full-pipe
959 (tunnel) flow? *Sedimentology*, 24(5):623-638
- 960 Schoof, C. (2010) Ice-sheet acceleration driven by melt supply variability. *Nature*, 468(7325): 803
- 961 Shreve, R. L. (1985). Esker characteristics in terms of glacier physics, Katahdin esker system,
962 Maine. *Geological Society of America Bulletin*, 96(5), 639–646.
963 [https://doi.org/10.1130/0016-7606\(1985\)96<639:ECITOG>2.0.CO;2](https://doi.org/10.1130/0016-7606(1985)96<639:ECITOG>2.0.CO;2)
- 964 Smith, M.J. and Knight, J. (2011) Palaeoglaciology of the last Irish Ice Sheet reconstructed from
965 striae evidence. *Quaternary Science Reviews*, 30(1-2): 147-160
- 966 Sollas, W.J. (1896) A map to show the Distribution of Eskers in Ireland. *Sci. Trans. R. Dublin Soc*,
967 2(5): 785-822.
- 968 Stearns, L.A., Smith, B.E. and Hamilton, G.S. (2008). Increased flow speed on a large East
969 Antarctic outlet glacier caused by subglacial floods. *Nature Geoscience*, 1(12), 827-831.
- 970 Storrar, R. D., Evans, D. J. A., Stokes, C. R., & Ewertowski, M. (2015). Controls on the location,
971 morphology and evolution of complex esker systems at decadal timescales,
972 Breidamerkurjökull, southeast Iceland. *Earth Surface Processes and Landforms*, 40(11),
973 1421–1438. <https://doi.org/10.1002/esp.3725>
- 974 Storrar, R.D., Ewertowski, M., Tomczyk, A.M., Barr, I.D., Livingstone, S.J., Ruffell, A., Stoker,
975 B.J. and Evans, D.J. (2020) Equifinality and preservation potential of complex
976 eskers. *Boreas*, 49(1), 211-231.
- 977 Storrar, R.D., Stokes, C.R. and Evans, D.J. (2013) A map of large Canadian eskers from Landsat
978 satellite imagery. *Journal of maps*, 9(3): 456-473
- 979 Storrar, R.D., Stokes, C.R. and Evans, D.J. (2014a) Morphometry and pattern of a large sample (>
980 20,000) of Canadian eskers and implications for subglacial drainage beneath ice
981 sheets. *Quaternary Science Reviews*, 105: 1-25

- 982 Storrar, R.D., Stokes, C.R. and Evans, D.J. (2014b) Increased channelization of subglacial drainage
983 during deglaciation of the Laurentide Ice Sheet. *Geology*, 42(3): 239-242
- 984 Stroeven, A. P., Hättestrand, C., Kleman, J., Heyman, J., Fabel, D., Fredin, O., Goodfellow, B. W.,
985 Harbor, J. M., Jansen, J. D., Olsen, L., Caffee, M. W., Fink, D., Lundqvist, J., Rosqvist, G.
986 C., Strömberg, B. & Jansson, K. N. (2016) Deglaciation of Fennoscandia. *Quaternary*
987 *Science Reviews*, 147, 91-121.
- 988 Walther, J. (1894) Einleitung in die Geologie als historische Wissenschaft. In *Lithogenesis der*
989 *Gegenwart*. Jena: G. Fischer, Bd. 3: 535–1055.
- 990 Warren, W.P. and Ashley, G.M. (1994) Origins of the ice-contact stratified ridges (eskers) of
991 Ireland. *Journal of Sedimentary Research*, 64(3a): 433-449
- 992 Wilson, P., Ballantyne, C.K., Benetti, S., Small, D., Fabel, D. and Clark, C.D. (2019) Deglaciation
993 chronology of the Donegal Ice Centre, north-west Ireland. *Journal of Quaternary Science*,
994 34(1): 16-28
- 995 Winsemann, J., Aspiron, U., Meyer, T. and Schramm, C. (2007) Facies characteristics of Middle
996 Pleistocene (Saalian) ice-margin subaqueous fan and delta deposits, glacial Lake Leine, NW
997 Germany. *Sedimentary Geology*, 193(1-4): 105-129
- 998 Winsemann, J., Hornung, J.J., Meinsen, J., Aspiron, U., Polom, U., Brandes, C., BUßMANN,
999 M.I.C.H.A.E.L. and Weber, C. (2009) Anatomy of a subaqueous ice-contact fan and delta
1000 complex, Middle Pleistocene, North-west Germany. *Sedimentology*, 56(4): 1041-1076
- 1001 Winsemann, J., Lang, J., Polom, U., Loewer, M., Igel, J., Pollok, L. and Brandes, C. (2018) Ice-
1002 marginal forced regressive deltas in glacial lake basins: geomorphology, facies variability
1003 and large-scale depositional architecture. *Boreas*, 47(4): 973-1002
- 1004 Wright, A. P., Siegert, M. J., Le Brocq, A. M., & Gore, D. B. (2008). High sensitivity of subglacial
1005 hydrological pathways in Antarctica to small ice-sheet changes. *Geophysical Research*
1006 *Letters*, 35(17), 1–5. <https://doi.org/10.1029/2008GL034937>
- 1007 Zwally, H.J., Abdalati, W., Herring, T., Larson, K., Saba, J. and Steffen, K. (2002) Surface melt-
1008 induced acceleration of Greenland ice-sheet flow. *Science*, 297(5579): 218-222